Korean J. Chem. Eng., 39(1), 20-37 (2022)
DOI: 10.1007/s11814-021-0947-5
pISSN: 0256-1115
eISSN: 1975-7220

INVITED REVIEW PAPER

Recent progress in dehydrogenation catalysts for heterocyclic and homocyclic liquid organic hydrogen carriers

Yeongin Jo*,‡, Jinho Oh,‡, Donghyeon Kim*, Ji Hoon Park**, Joon Hyun Baik***,†, and Young-Woong Suh*,****,†**

*Department of Chemical Engineering, Hanyang University, Seoul 04763, Korea
**Center for Environment & Sustainable Resources Research,
Korea Research Institute of Chemical Technology, Daejeon 34114, Korea
***Department of Chemical and Biological Engineering, Sookmyung Women's University, Seoul 04310, Korea
****Research Institute of Industrial Science, Hanyang University, Seoul 04763, Korea
(*Received 18 July 2021 • Revised 24 August 2021 • Accepted 31 August 2021*)

Abstract−Liquid organic hydrogen carriers (LOHC) are recently recognized as an attractive solution for H_2 storage and transportation. Among several challenging tasks for practical application, the most stringent limitations stem from the dehydrogenation reaction requiring high temperatures thermodynamically. Unlike previous reviews focusing on the LOHC concept, LOHC molecules, and process integration, this review highlights the state-of-the-art catalysts reported for the dehydrogenation of homocyclic and heterocyclic LOHC molecules. In the conversion of heterocyclic LOHC, Pd-based catalysts overnumbered Pt-based ones owing to preferential adsorption of heteroatoms onto the Pd surface. However, because of low stability of C-heteroatom bonds, catalyst development needs to concentrate on inhibiting the generation of byproducts while maintaining superior performance under mild conditions. In the case of homocyclic LOHC, Pt is overwhelmed in single metal and bimetallic catalysts owing to pronounced C-H bond cleavage. Nevertheless, the ability of Pt in C-C bond cleavage should be diminished for higher H_2 selectivity, better catalyst stability, and steady LOHC recyclability, which is possible by tuning electronic and geometric effects of main active metals, as well as adding metal promoters. Consequently, great efforts will be diversely devoted to achieving an active and stable dehydrogenation catalyst for future LOHC demonstration.

Keywords: Liquid Organic Hydrogen Carriers, Dehydrogenation, Heterogeneous Catalysts

INTRODUCTION

Use of fossil fuels has been increasing because of soaring energy demand in recent decades, imparting negative effects on the global environment by greenhouse gases emitted in use. Thus, humanity worldwide is facing regulations to reduce greenhouse gas emission from 2020 according to the Paris Agreement adopted in 2015 United Nations Climate Change Conference. Many countries have devoted themselves to replacing the previous energy sources with renewable energy (e.g., solar, wind, geothermal, bioenergy, etc.) in order to achieve their own goals [1,2]. Hydrogen energy among them is being discussed as a promising candidate with the most ideal potential to emit small pollutants [3]. It is, hence, essential to solve various problematic issues in the sectors of hydrogen generation, storage and transportation, and utilization so as to realize the hydrogen economy system in the future [4,5].

Hydrogen has a high gravimetric energy storage density of 33.6 kWh per kg, but a extremely low volumetric storage density of 3 Wh per liter at STP [6]. Also, it cannot be easily handled due to gas phase and flammability. These make it difficult to transport and use hydrogen gas, so that researches are currently underway in various technical fields for hydrogen storage [7-9]. The most widely used storage method is compressed hydrogen and liquefied hydrogen. These two types have the advantages of utilizing the existing pipeline infrastructure and not requiring additional materials; however, the cost and electricity to make and maintain each state are too high to store it efficiently [10]. There are another storage methods such as physical adsorption in porous materials with high surface areas and metal hydrides, where the former has poor storage efficiency [9] and the other also has difficulties in transporting a solid material and securing the stability of H_2 storage and release due to thrmal decomposition [11,12]. Compared with the aforementioned methods, the concept of liquid organic hydrogen carriers (LOHC), which are high-boiling organic molecules and reversibly hydrogenated and dehydrogenated, has many advantages in stability, non-flammability, and management [13].

LOHC molecules are classified into two groups depending on the presence of heteroatoms (i.e., N, S, O, and B) in the molecular structure. Homocyclic LOHC includes cyclohexane, methylcyclohexane (MCH), decalin, bicyclohexyl, perhydrobenzyltoluene (H_{12}-MBT), and perhydrodibenzyltoluene (H_{18}-DBT). Although the dehydrogenation mechanism is similar to that of heterocyclic LOHC, homocyclic one does not contain elements positively affecting the dehydrogenation reaction from a viewpoint of molecular structure. Also, the bond between carbon and heteroatoms does not need to

†To whom correspondence should be addressed.
E-mail: joonhyun@sookmyung.ac.kr, ywsuh@hanyang.ac.kr
‡Equal contribution.

be cleaved by catalytic functions; thus, side reactions involving heteroatoms can be neglected. Heterocyclic LOHC molecules are developed to reduce the energy required for the dehydrogenation of homocyclic LOHC ($\Delta H_{dehydro}$>60 kJ mol_{H2}^{-1} [14,15]). A well-known example is *N*-ethylcarbazole (NEC) capable of low-temperature H_2 release at below 200 °C [16-18], thus attracting considerable attention owing to favorable kinetics and low dehydration temperatures [16,19-23]. However, it has two main drawbacks to complicate implementation for practical applications: a) the fully dehydrogenated, pure NEC is a solid at room temperature (m.p. 68 °C) [24], b) the thermal stability of NEC is limited by the dealkylation to carbazole possibly happening at above 270 °C in the presence of catalysts. Thus, various N-heterocyclic LOHC molecules are studied: for instance, indoles and alkyl-substituted indoles, phenazine, and perhydro-4,7-phenanthroline.

Despite the merits of LOHC, it has not been commercialized yet because of high hurdles in the dehydrogenation reaction regarded as the bottleneck of this storage method [10]. Specifically, the reaction temperature (200-350 °C) is so high due to endothermic nature while the reaction rate is relatively low, so that many side reactions possibly occur and it is difficult to achieve full conversion [25]. Moreover, expensive, noble metal catalysts are commonly used. Nevertheless, there are sufficient possibilities for commercialization if one can overcome these challenges through intensive efforts in academia and industry [13]. There are three general strategies to complete adequate, fast, and cheap hydrogen release: 1) process development, 2) new LOHC molecules, and 3) catalyst modification. As the first representative, Wasserscheid et al. [26] suggested a reactor of reactive distillation to cut off the H_2-lean molecule inhibiting the dehydrogenation reaction rate and thereby make the H_2-rich molecule in facile contact with the dehydrogenation catalyst. A typical example in the second strategy was reported by Suh and coworkers [27] that a new heterocyclic LOHC, 2-(*n*-methylbenzyl)pyridine (MBP), was designed by adding N atom into the benzene ring of *n*-benzyltoluene based on density functional theory (DFT) calculation. This molecule of H_2-rich form showed much faster hydrogen release over Pd/C than the benzyltoluene counterpart over Pt/C and was stable in a few of recycle tests. In terms of catalyst modification, Wang et al. [28] discussed an effect of facet structure on the rate-determining step in the dehydrogenation of dodecahydro-*N*-ethylcarbazole and recommended to control the facet of Pd particles in the design of the Pd/rGO catalyst. Aside from the above examples, various efforts are continuing to go beyond the limitations of the dehydrogenation reaction.

Recent reviews mostly focused on the LOHC technology, and partly on the catalytic dehydrogenation process and integration with fuel cells [13,29-32]. This review deals with the state-of-the-art dehydrogenation catalysts for heterocyclic and homocyclic LOHC molecules, though previously summarized in part. For homocyclic LOHC, Pt is the most common active metal and catalyst works have been actively conducted with focus on the conversion, selectivity, reaction rate, activation energy, and stability. In the dehydrogenation of heterocyclic LOHC, Pd exhibits a better activity than Pt [27,33,34], where catalyst stability is also important because of strong adsorption of heteroatoms onto active metals [35]. Although desired catalytic functions depend on the structure of the tested LOHC molecule, they can be discussed in similar factors for high activity and selectivity. Thus, the context is based on the type and

Table 1. Examples of single Pt catalysts reported for LOHC dehydrogenation

Active metal	Promotor	Support	Preparation method	Reactant	Reaction temperature (°C)	Reactor type	Results[a]	Ref.
Pt	-	TiO_2	Ion exchange	Cyclohexane	270	Batch	TOF=0.70 s^{-1}	37
		TiO_2	Solvent-thermal reduction	NEC	180	Batch	TOF=259.73 min^{-1} H_2 yield=99.3% S to *N*-ethylcarbazole=98.0%	75
	-	C	Impregnation	Decalin	250 to 270	Batch	X=69% at 270 °C S to naphthalene=68.4% at 270 °C	34
	-	AC	Impregnation	Decalin	300	Continuous	X=85% S to naphthalene=95%	38
	-	C	Impregnation	Decalin	200	Batch	27.8 $mmol_{H2}$ h^{-1} at 2.5 h X=26.5% at 2.5 h	39
	-	AC	Impregnation	Decalin	280	Liquid-film state	400.0 $mmol_{H2}$ h^{-1} X>95.0% within 1.5 h	40
	-	AC	Impregnation	Decalin	210	Batch	6 $mmol_{H2}$ for 150 min	41
	-	ACC	Impregnation	Decalin	280	Liquid-film state	34 $mmol_{H2}$ for 1 h X=92% at 1 h	42
	-	CNTs	Impregnation	Decalin	196.6	Batch	320.5 mol_{H2} h^{-1} mol_{Pt}^{-1} S to naphthalene=70.2%	43
	-	ACA	Impregnation	Decalin	210	Batch	450 $mmol_{H2}$ g_{Pt}^{-1}	44

Table 1. Continued

Active metal	Promotor	Support	Preparation method	Reactant	Reaction temperature (°C)	Reactor type	Results[a]	Ref.
Pt	-	CB	Impregnation	MCH	300	Continuous	X>95% S to toluene=100%	45
	-	CNFs	Deposition-precipitation	Decalin	240	Liquid-film state	732.4 mol_{H2} mol_{Pt}^{-1} for 2 h X=46.3% S to naphthalene=93.2%	46
	-	CNFs	HCHO reduction	Decalin	240	Batch	729.9 mol_{H2} mol_{Pt}^{-1} for 2 h X=60.2% S to naphthalene=97.1%	47
	-	CNFs	Impregnation	Decalin	260 to 360	Continuous	55.4 $mmol_{H2}$ g_{Pt}^{-1} min^{-1}	48
	-	C	Ion exchange	Decalin	210	Batch	333.3 $mmol_{H2}$ g_{Pt}^{-1} for 60 min	49
	-	CNFs	Ion exchange	Decalin	240	Batch	2,500 $mmol_{H2}$ g_{Pt}^{-1} for 120 min X=35% at 100 min	50
	-	C	Impregnation	Decalin	240 to 260	Batch	X=55% S to naphthalene=95%	51
	PhTES	CB	Impregnation	Cyclohexane	250	Continuous	X=47%	52
	HNO_3	MWNT	Impregnation	Decalin, cyclohexane	225	Continuous	TOF of decalin=1.96 min^{-1} TOF of cyclohexane=25.0 min^{-1}	53
	N	CNFs	Impregnation	Decalin	230	Batch	14.0 $mmol_{H2}$ m^{-2} Pt h^{-1}	54
	N	CNT	Impregnation	Decalin	230	Batch	1,000 $mmol_{H2}$ g_{Pt}^{-1} min^{-1} at 30 min	55
	N	C	Impregnation	Cyclohexnae	210	Batch	X=96.0% at 90 min	56
	-	Al_2O_3	Impregnation	Cyclohexane	270	Continuous	71.3 μmol_{H2} s^{-1} g_{cat}^{-1}	58
	-	Al_2O_3	Ion exchange imp.	NEC	220 to 260	Continuous	TOF=17.5 mol_{H2} mol_{Pt}^{-1} s^{-1} H_2 yield=20.9%	77
	CaO	γ-Al_2O_3	Impregnation	Cyclohexnae	300	Continuous	X=87% at 1 h	59
	Ca	γ-Al_2O_3	Impregnation	Cyclohexane	300	Continuous	Initial activity=87%	60
	S	Al_2O_3	Impregnation	DBT	310	Batch	H_2 yield=80% at 40 min	61
	S	Al_2O_3	Impregnation	DBT	310	Batch	4.3 g_{H2} g_{Pt}^{-1} min^{-1} at initial state	62
	-	Al_2O_3	Impregnation	DBT	270	Batch	H_2 yield=70% at 300 min	63
	TiO_2	Al_2O_3	Impregnation	MCH	400	Continuous	1,711 mol_{H2} mol_{Pt}^{-1} h^{-1} X=93.2% S to toluene=99.1%	64
	-	TiO_2	Impregnation	MCH	350	Continuous	H_2 yield=65.6% at 420 min	65
	TiO_2	Al_2O_3	Impregnation	MCH	335	Continuous	X=95% CH_4 concentration=75 ppm	66
	-	TiO_2	Impregnation	MCH	175	Continuous	X=37%	67
	-	CeO_2	Impregnation	MCH	150	Continuous	H_2 yield=21.6%	68
		SBA-15	Co-assembly	MCH	300	Continuous	X=65.0% S to toluene=~100% Higher stability	69
	TiO_2	SBA-15	Impregnation	Cyclohexane	270	Continuous	Higher SMSI effect	70
	-	$La_{0.7}Y_{0.3}NiO_3$	Co-precipitation	MCH	350	Spray-pulsed	45.8 $mmol_{H2}$ g_{Pt}^{-1} min^{-1} at 90 min	71
	-	Y_2O_3	Impregnation	MCH	350	Spray-pulsed	958 $mmol_{H2}$ g_{Pt}^{-1} min^{-1} at 60 min	72

[a]X=conversion, S=selectivity

kind of active metals. First, the works on single metal catalysts are described in terms of catalyst functions in the order of Pt, Pd, and other metals (Ir, Co, Cu, Mo, Nb, and Ni). Then, bimetallic catalysts containing Pt or not are introduced. Finally, directions will be discussed toward finding an active dehydrogenation catalyst.

SINGLE METAL CATALYSTS

1. Pt Catalysts

In the dehydrogenation of homocyclic LOHC, the cleavage of C-H bonds must occur all around without breaking C-C bonds. Pt is a well-known metal in rupturing the C-H bond with the highest capability. The representative Pt catalysts are listed in Table 1. Kim et al. [34] found the conversion of decalin to tetralin to be more energetically beneficial on Pt than on Pd by DFT calculation. However, Pt is also active in cleavage of the C-C bond as used in traditional catalytic reforming. The activity of Pt catalysts is largely determined by the particle size [36] and support acidity [37], depending on the characteristics of supports including carbon and metal oxides. Also, these catalyst properties can be tuned by a method of metal loading, support modification, and dopant addition.

Carbon is a representative high-surface-area support that exists in various derivatives including activated carbon (AC), carbon black (CB), carbon aerogel (CA), carbon nanofiber (CNF), carbon nanotube (CNT), graphene oxide (GO). It is also the most studied in Pt-based catalysts. For instance, Pt/AC was superior to Pt/Al_2O_3 in decalin dehydrogenation owing to both high Pt dispersion and hydrogen spillover [38]. In several studies on carbon supported Pt catalysts was termed "superheated liquid-film state" where catalyst particles were not suspended in a reaction mixture all through the dehydrogenation process. Using this concept, Pt/AC showed rapid dehydrogenation of decalin and the activity critically depended on the mass ratio of decalin to catalyst [39-42]. Subsequent studies revealed that the catalyst state is beneficial in both H_2 diffusion and desorption of aromatic products blocking active sites.

A variety of carbon supports are used for Pt catalysts. Li et al. [43] prepared Pt catalysts supported on graphite, AC, CB, CNF, and CNT. When tested in decalin dehydrogenation under microwave irradiation (MW), Pt/CNT was found to be the most active owing to high Pt dispersion and low bulk density. On the other hand, activated carbon aerogel (ACA), prepared by KOH treatment and thermal activation at 800 °C for 2 h under N_2, was reported to be a better support than AC and CA for Pt-catalyzed decalin dehydrogenation [44]. There was the case using pyrolytic waste tire char for Pt catalyst in MCH dehydrogenation [45]. Also, CNFs with microstructure types of tube (t-CNF), fishbone (f-CNF), and platelet (p-CNF) were parepared by chemical vapor deposition (CVD) and used as a support of Pt catalyst for decalin dehydrogenation [46]. As a result of activity test at 240 °C, 5 wt% Pt/p-CNF exhibited a higher TOF of of 732.4 mol_{H2} mol_{Pt}^{-1}. Additionally, when Pt/CNF was activated by formaldehyde reduction, Pt species was completely converted to Pt^0 without increasing the particle size and showed an outstanding activity of 729.9 mol_{H2} mol_{Pt}^{-1} [47]. The activity of these Pt catalysts was discussed in terms of Pt particle size, metal-support interaction, and diffusion limitation: a fibrous structure of CNF was advantageous to both external and internal diffusion [48].

The synthesis method for Pt/C catalysts was modified to increase Pt dispersion playing a key role in decalin dehydrogenation. With regards to initial hydrogen release rate and total amount of hydrogen evolution, ion exchange and polyol methods afforded the active Pt catalysts [49]. In case of Pt loading, 4 wt% Pt was optimal at obtaining a specific Pt particle size for the best hydrogenation activity [50]. To promote the metal-support interaction, Pt/CNF was prepared by ion exchange of the cationic Pt precursor with the protons of oxygenated functional groups in the CNF surface [51]. This catalyst contained well dispersed Pt particles of about 2 nm and represented four-fold higher H_2 production than Pt/AC.

Carbon derivatives are modified to locate silica and oxygen or nitrogen functional groups at the surface. Nakagawa et al. [52] reported a Pt/CB catalyst coated with microporous silica layers was obtained using phenyltriethoxysilane followed by thermal treatment at 973 K. SiO_2-coated Pt/CB showed a higher conversion than pristine Pt/CB in cyclohexane dehydrogenation, because the large micropore of silica layer enhanced the diffusion of cyclohexane for the reaction. On the other hand, multi-walled carbon nanotubes (MWNT) to improve Pt dispersion were treated with nitric acid, yielding oxygen-containing groups [53]. This surface modification did not affect TOF of alkane dehydrogenation, but did have a geometric effect on the dehydrogenation performance becuase transportation limitations were more evident in the larger decalin than the smaller cyclohexane. Likewise, partial oxidation for Sibunit support catalyzed bicyclohexyl dehydrogenation more effectively than the parent one for Pt catalyst [48]. For improved activity in decalin dehydrogenation, defect types such as doped nitrogen and edge-like sites were introduced into the three types of CNFs [54]. The Pt/p-CNF with defect sites developed showed the most adequate metal-support interaction and thereby the high performance. New edge-like defects, generated by thermal treatment removing nitrogen compounds, worked beneficially on the supports of t-CNF and f-CNF (Fig. 1(a)). In Pt catalyst supported on nitrogen-doped carbon, the activity in cyclohexane dehydrogenation was in a volcano-type relationship with the Pt particle size of between 1.6 and 3.1 nm [55]. Furthermore, the effects of surface modification by oxygen and nitrogen groups were investigated on the decalin dehydrogenation activity [56]. Although the oxygen functional groups helped Pt dispersion, they were found to reduce the adsorption energy of decalin by inhibiting electron transfer from Pt to carbon support. However, the nitrogen functional groups on Pt/CNF led to higher Pt dispersion, positively charged Pt, and non-polar catalyst surface. These resulted from the enhanced electron transfer from Pt to CNF by the nitrogen group (Fig. 1(b)).

Also, metal oxides as support are known to have hydrogen spillover and thermal stability. Particularly, hydrogen spillover aiding dehydrogenation is preferred over metal oxides because of low energy barrier and thermodynamic properties [57]. The metal oxides usually employed for Pt catalysts are Al_2O_3, TiO_2, CeO_2, SiO_2, La_2O_3, V_2O_5, Y_2O_3. In LOHC dehydrogenation, state-of-the-art works with these supported Pt catalysts focused on the effects of support's characteristics and modification on catalytic activity and product selectivity.

The activity of Pt/Al_2O_3 cyclohexane dehydrogenation is well

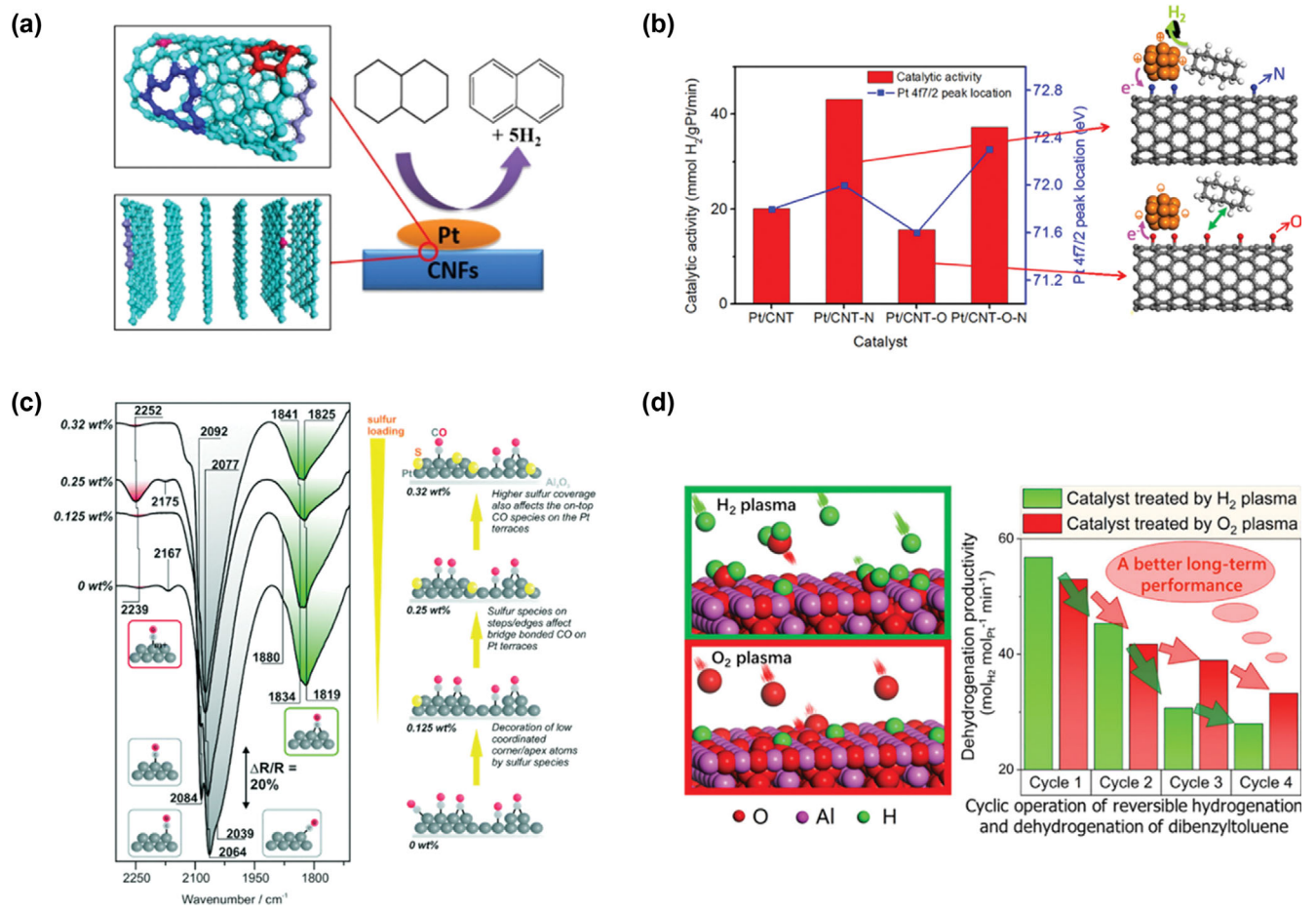

Fig. 1. Key findings of single Pt catalysts in literature. (a) Schematic of edges and edge-like defects in Pt/CNFs (Reproduced with permission from Ref. [54], Copyright 2018, Elsevier). (b) Electron transfer effect in Pt/CNT (Reproduced with permission from Ref. [55], Copyright 2020, Elsevier). (c) CO-DRIFTS results with respect to sulfur loading on Pt/Al_2O_3 (Reproduced with permission from Ref. [61], Copyright 2018, Royal Society of Chemistry). (d) Effect of the plasma treatment on the dehydrogenation performance under cyclic operation (Reproduced with permission from Ref. [63], Copyright 2020, American Chemical Society).

correlated with Pt dispersion: for example, the catalyst with 0.5 wt% Pt showed the Pt dispersion of 76% as well as the highest activity [58], which was also found in other supports. While Al_2O_3 has been used widely, it is sometimes modified for activity enhancement. In case of CaO-modified Al_2O_3, highly dispersed Pt was achieved by promotional effects of Ca-Al interaction and larger CaO particles, resulting in lower acidity and more H_2 spillover [59]. This enhancement reached a maximum at the Ca/Pt ratio of 5, leading to outstanding activity and stability [60]. Another example was sulfur modified Pt/Al_2O_3 for fast DBT dehydrogenation kinetics [61]. Sulfur atoms could be preferentially adsorbed to defect sites (i.e., edges or corner/apex) of Pt particles, inhibiting side reactions and further improving the reaction rate and selectivity (Fig. 1(c)). Additionally, Pt particle size was optimized to decrease the formation of side products (e.g., high boiler) in DBT dehydrogenation [62]. At the optimal amount of sulfur, the catalytic activity was the highest with Pt size of 1.55 nm and side reactions were the most suppressed.

Shi et al. [63] investigated the effects of surface hydroxyl groups (SHG) and surface oxygen vacancies (SOV) created by H_2 and O_2 plasma treatment for Pt/Al_2O_3 catalyst, respectively. Both treatments enhanced Pt dispersion. Particularly, the SHG improved the reactivity and stability by increases in the Pt^0 proportion and H_2 spillover, whereas the SOV provoked side reactions by enriching the low-coordinated Pt defect sites to have a negative effect on the dehydrogenation productivity under cyclic operation (Fig. 1(d)). Therefore, key points in Al_2O_3 modification are to boost the SHG and appropriately reduce the SOV for DBT dehydrogenation.

Titanium oxide (TiO_2) can transfer electron to Pt metal, which is distinguished from other supports. To reduce weak acid sites and increase the electron density of Pt, TiO_2 was added into Al_2O_3 and the resulting Pt/TiO_2-Al_2O_3 with 10 wt% TiO_2 exhibited the highest Pt dispersion for MCH conversion [64]. Furthermore, Sekine et al. [65,66] observed that the reaction order was almost zero with respect to the partial pressure of toluene in MCH dehydrogenation over Pt/TiO_2, meaning that the dehydrogenation rate is hardly affected by the inhibition of toluene adsorption, unlike Al_2O_3. This was explained by electron donation of TiO_2 leading to electron-rich Pt species that could weaken the adsorption strength of toluene. Such an effect of TiO_2 was maximized by activation of sup-

ported Pt on TiO_2 of anatase phase under an electric field to generate surface protonics, thus obtaining the improved MCH conversion of 37% at 448 K [67]. The electric field also enabled to lower the activation energy by nearly half that in no electric effect. This strategy related to the surface protonics was also demonstrated in CeO_2 support [68]. In case of Pt/CeO_2 with the lower surface area and smaller pore size that Pt/Al_2O_3, a combustion method, such as glycine nitrate process, was developed to overcome mass transfer limitations, which was effective in H_2 release from DBT [69].

Mesoporous silica was also used as support for Pt loading. A one-pot co-assembly synthesis was applied for encapsulating highly dispersed Pt particles into the mesochannels of SBA-15 [70]. The growth of Pt nanoparticles was hindered due to the restriction effect of the mesochannels, showing improved catalytic stability in MCH dehydrogenation. As a similar concept, Pt nanoparticles sandwiched between SiO_2 core and mesoporous SiO_2 shell were synthesized as a more stable and active catalyst than conventional Pt/SiO_2 in cyclohexane dehydrogenation [71]. This catalyst did not only exhibit the outstanding thermal stability but also was regenerated at high temperatures. On the other hand, TiO_2 nanoclusters were integrated with a mesostructured SiO_2 support for Pt loading [72]. Owing to controlling of titania crystal size, the strong metal-support interaction (SMSI) effect of TiO_2 could be appropriately changed and thereby lead to enhancement of the dehydrogenation activity.

Various metal oxides (La_2O_3, Al_2O_3, CeO_2, MnO_2, TiO_2, Fe_2O_3, and ZrO_2) were used as support for Pt catalyst in MCH dehydrogenation [73]. In terms of H_2 evolution rate, the support ranked in the following sequence: $CeO_2<ZrO_2<MnO_2<Fe_2O_3<Al_2O_3<TiO_2<La_2O_3$. 3 wt% Pt/La_2O_3 had the largest particle size of 9.81 nm, but afforded the best performance due to facilitated H_2 spillover. In a series of works, the activities of Pt/V_2O_5 and Pt/Y_2O_3 were compared with that of Pt/Al_2O_3 in a spray-pulsed reactor [74]. 3 wt% Pt/Y_2O_3 showed excellent activity (958 $mmol_{H2}$ g_{Pt}^{-1} min^{-1}) in MCH dehydrogenation. Once again, well dispersed Pt particles and H_2 spillover proved to be pivotal in this catalyst system.

In the dehydrogenation of heterocyclic LOHC, Pt is less used because the dehydrogenation activity is so high that side reactions such as disproportionation, dealkylation, and C-heteroatom bond cleavage can occur. When Pt/TiO_2 (optimal Pt loading: 1 wt%) was applied for H_{12}-NEC dehydrogenation [75], the hydrogen release amount and H_0-NEC selectivity were estimated to be 5.75 wt% and 98% at 180 °C, respectively. The activity and stability were higher than 5 wt% Pd/Al_2O_3 and Pt/Al_2O_3. Ti^{4+} tended to be partially reduced by Pt deposition and vacant sites were generated around Pt [76]. Therefore, the superior catalytic performance of Pt/TiO_2 was associated with the SMSI effect between Pt and TiO_2, and the vacancies of TiO_2 as well. On the other hand, the effects of pore diffusion were studied by using an egg-shell catalyst, Pt/γ-Al_2O_3 layer on α-Al_2O_3 core of different active layer thicknesses (24 to 88 μm) deposited via ion exchange of a H_2PtCl_6 solution [77]. Even at a very thin layer of 24 μm, the kinetic regime was limited to 235 °C and thus pore diffusion strongly affected the dehydrogenation reaction rate. The catalyst with the active layer of 33 μm exhibited a remarkable productivity of up to 10.9 g_{H2} g_{Pt}^{-1} min^{-1} at 262 °C, corresponding to H_2 release efficiency of 20.9% and turnover frequency (TOF) of 17.5 mol_{H2} mol_{Pt}^{-1} s^{-1}.

Table 2. Examples of single Pd catalysts reported for LOHC dehydrogenation

Active metal	Promotor	Support	Preparation method	Reactant	Reaction temperature (°C)	Reactor type	Results[a]	Ref.
Pd	-	SiO_2	Sol-gel	Indoline	100	Batch	X=~81%	78
	-	SiO_2	Impregnation	NEC	170	Batch	TOF=221.16 min^{-1} S to *N*-ethylcarbazole=94.8% at 1 h	80
	-	rGO_{-EG}	Ion exchange	NEC	170	Batch	H_2 yield=94.7% at 12 h S to *N*-ethylcarbazole=84.6% at 12 h	82
	-	C	Commercial	NEC	180	Batch	H_2 yield=98.1% at 12 h X=90.5% at 1 h S to *N*-ethylcarbazole=35.5% at 1 h	83
	-	HAP (hydroxyapatite)	Impregnation	Indoline	100	Batch	TOF=~2,800 h^{-1} H_2 yield>99% at 1 h X>99% at 1 h	84
	-	CCA	Impregnation	MBP	250	Batch	H_2 yield=71.1% X=80.6% S to H_0-MBP=76.4%	87
	-	Al_2O_3	Solvent-deficient precipitation	MBP	250	Batch	H_2 yield=70.4% X=80.2% S to H_0-MBP=75.4%	88, 89
	-	C	Commercial	Phenyl-cyclohexyl	250	Liquid-film state	Higher X than Pt	71

[a]X=conversion, S=selectivity

2. Pd Catalysts

In the dehydrogenation of heterocycles without substrate degradation, especially when an alkyl protecting group is present on the heteroatom, the activity generally follows in the order: Pd>Pt>Ru>Rh. Therefore, Pd catalysts are the most widely studied dehydrogenation catalysts for heterocyclic LOHC because of high activity at low temperatures (Table 2). Pd catalysts showed 100% selectivity toward H_0-NEC at complete conversion [78,79]. Sotoodeh et al. [80] found that Pd/SiO_2 fully dehydrogenated H_{12}-NEC within 1.6 h at 170 °C. This resulted from preferential adsorption of N atom onto the Pd surface because the dehydrogenation efficiency of perhydrocarbazole was much lower over Pt catalyst under the same conditions (Fig. 2(a)). Moreover, the reaction rate and selectivity of H_0-NEC depended on the size of Pd particles. The dehydrogenation efficiency reached the highest (4 wt%) at 170 °C when the Pd size was about 9 nm [81]. This indicates that the adsorption energy of H_{12}-NEC is related to the surface structure of Pd nanoparticles.

Wang et al. [82] reported the performance of a reduced graphene oxide (rGO) supported Pd catalyst prepared by one-pot synthesis using ethylene glycol. The specific activity of Pd/rGO in the dehydrogenation of H_{12}-NEC significantly increased up to 14.4 times, even though the Pd amount was only half of commercial 5 wt% Pd/Al_2O_3 catalyst. With 2.5 wt% Pd/rGO, the dehydrogenation efficiency was measured to be 5.27, 5.49, and 5.78 wt% at 160, 170, and 180 °C for 12 h, respectively. The benefits of rGO support could be classified into three categories: 1) It has high surface area, good adsorption property, strong mechanical strength, excellent stability and conductivity. 2) The planar two-dimensional electronic structure facilitates the modification of various molecules and atoms. 3) The surface of rGO contains many active groups and defects to adsorb and anchor metal nanoparticles. Furthermore, the authors highlighted the Pd(111) facet in the enhanced performance of Pd/rGO catalyst as shown in Fig. 2(c) [28].

Therefore, the support properties certainly affect the dehydrogenation efficiency of Pd catalysts. Feng et al. [83] studied the dehydrogenation kinetics of four supported Pd catalysts such as Pd/C, Pd/Al_2O_3, Pd/TiO_2, and Pd/SiO_2. In case of Pd/C, the Pd size was averaged at 3.0 nm, the specific surface area was 1,754 $m^2\ g^{-1}$, and the reduction degree of Pd was 32.1%. As a result, Pd/C showed a higher initial rate constant of 0.0086 min^{-1} than the other tested catalysts. This suggests that the structure, particle size, and reduction degree of Pd as well as textural properties of support have a synergistic effect on catalytic performance. On the other hand, Hara et al. [84] reported that a hydroxyapatite ($Ca_{10}(PO_4)_6(OH)_2$) supported Pd catalyst (Pd-HAP) was highly efficient in the dehy-

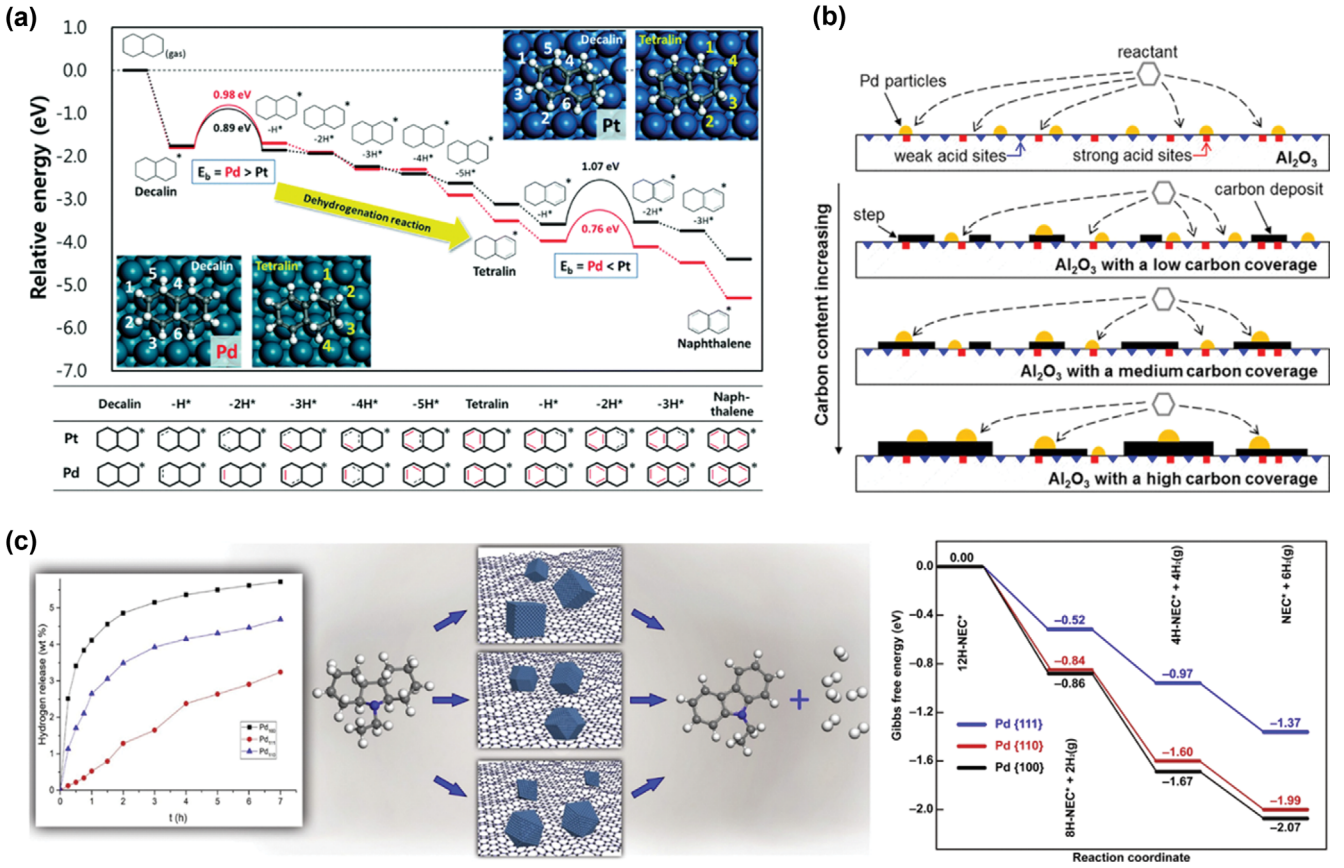

Fig. 2. Key findings of single Pd catalysts in literature. (a) Relative energy diagram for the dehydrogenation of decalin on Pd(111) and Pt(111). (b) Schematic for the proposed model to support the activity and stability of Pd/CCA catalysts. (c) Activity and Gibbs free energy results in the H_{12}-NEC dehydrogenation over different Pd facets such as (100), (110), (111) (Reproduced with permission from Ref. [28], Copyright 2010, Elsevier).

drogenation of various indoline derivatives [85]. Pd-HAP catalyzed the dehydrogenation of all the tested indolines to the corresponding indoles at high yields (>97%). Even sterically hindered indolines such as carbazoline, N-benzylindoline, and 2-phenylindoline were converted at the yield of 94%, 92%, and 92%, respectively. From the Pd-HAP isolated from the reaction mixture, Pd nanoparticles were sized at diameters of ca. 9 nm, revealing that Pd^{2+} species are reduced to Pd^0 under the reaction conditions and dehydrogenation occurs on the Pd particles on the HAP surface. According to the reaction mechanism, the N atom of indoline would be coordinated to the Pd^0 species, followed by oxidative addition to the N atom to produce σ-alkyl Pd intermediate species and subsequent β-hydride elimination, affording the corresponding indole and Pd^0 along with H_2 evolution.

Besides catalytic activity, the stability of supported Pd catalysts in recycle runs is challenging in LOHC dehydrogenation. Referring to good stability of carbon-coated alumina (CCA) in hydroprocessing reactions [86], Oh et al. [87] prepared Pd/CCA catalysts by pyrolysis of aqueous glycerol solutions with different concentrations. When they were tested in the dehydrogenation of 2-[(*n*-methylcyclohexyl)methyl]piperidine (H_{12}-MBP), the activity and stability exhibited a volcano-shaped relationship with the carbon content. Indeed, the degree of carbon coating affected the support acidity, Pd loading and particle size, and adsorption capacity of the reactant. At the optimal carbon content of 3.3 wt% (Pd/3.3CCA), these properties were well balanced, thus affording the best performance such as H_{12}-MBP conversion of 80.6% and H_0-MBP selectivity of 76.4% at 250 °C for 4 h. Moreover, the improved stability of Pd/3.3CCA orginated from the carbon deposits being able to lower the sintering ability of Pd (Fig. 2(b)). In a successive work for the dehydrogenation of H_{12}-MBP, the one-pot solvent deficient precipitation (SDP) was suggested to synthesize an active and stable Pd catalyst [88]. The mesoporous Pd-Al_2O_3 catalyst (MPdA) with 1 wt% Pd offered outstanding H_2 release capability compared to conventional Pd counterparts in N-heterocyclic molecules including H_{12}-NEC and H_{12}-MBP. Moreover, the robustness of MPdA was confirmed by negligible activity loss up to five consecutive dehydrogenation runs of both H_{12}-MBP and perhydro-2-methylindole (H_8-MID). Such outstanding performance of MPdA was considered to possibly result from the solvent deficient environment in the synthesis restricting the mobility of Pd particles by contiguous Al_2O_3 particles and producing well-dispersed Pd phase with a higher density of Pd (111) plane. The sensitivity and effectiveness of the SDP method were also examined by changing the calcination condition [89]. Therefore, new catalyst preparation methods are worth being further exploited for innovative dehydrogenation catalysts.

Metal-support interaction of supported Pd catalysts is determined by the intrinsic surface characteristics of each metal oxide [90] and will greatly affect the performance (H_2 yield and reaction rate) of Pd nanoparticles [83,91-93]. Kim et al. [94] recently studied the activity of Pd catalysts (5 wt% Pd) supported on Al_2O_3, CeO_2, TiO_2, ZrO_2, and SnO_2 in the dehydrogenation of H_{12}-MBP. The H_2 yield and reaction rate were correlated with the surface characteristics of metal oxide, such as acidity, adsorption affinity, and charge transfer of H_{12}-MBP. Particularly, Pd/Al_2O_3 outperformed the other catalysts in the following order: Pd/Al_2O_3>Pd/CeO_2>Pd/TiO_2>Pd/ZrO_2>Pd/SnO_2. Pd/Al_2O_3 showed the Pd mean size of 5.8 nm and the highest H_2 yield of 75.8%, whereas Pd/CeO_2 did the lower H_2 yield (67.1%) and slower reaction rate even though it had the highest reducibility, the best support ability for Pd nanoparticles, and the smallest Pd mean size of 3.5 nm. However, the best recyclability was obtained with Pd/CeO_2, suggesting strong metal-support interaction of Pd with CeO_2.

On the other hand, Pd catalysts are not popular for homocyclic LOHC due to the high activity of Pt. Ninomiya et al. [95] compared the activities of Pt and Pd catalyst supported on carbon. Pt was more active than Pd in dicyclohexyl dehydrogenation. However, Pd showed a higher conversion than Pt in the dehydrogenation of phenyl-cyclohexyl intermediate because the reactant with an aromatic ring tended to promote Pd activity, which is linked to prevalence of Pd in the dehydrogenation of heterocyclic compounds. According to the simulation results performed with Pd supported on Al_2O_3 or sapphire catalysts for MCH dehydrogenation [96], a phase of Pd particles depended on the presence of hydrogen. In the case of Pd/Al_2O_3, α-PdH and β-PdH phases were formed as a transition state. β-PdH formed at 300 K disappeared as the temperature rose, resulting in the decline in the conversion. On sapphire support, hydrogen deficiency led to formation of PdC_x and bulk carbon was less formed under H_2 atmosphere. These explained the stability of Pd catalysts based on the characteristic of H_2 release.

3. Other Single Metal Catalysts

Except single Pt and Pd catalysts, Ir and several non-noble metal catalysts are applied for the dehydrogenation of homocyclic LOHC (Table 3). Among metal catalysts supported on zeolite USY, the MCH conversion and H_2 selectivity were much higher with Ir/USY and decreased in the following order: Ir/USY>>Pt/USY>Pd/USY>Ni/USY [97]. Moderate metal-support interaction found in Ir/USY induced the formation of larger Ir particles, contributing to the high activity because of fewer hydrogenolysis sites.

Non-noble metal catalysts are studied for LOHC dehydrogenation because they are quite cheap, although the intrinsic activity would be lower compared to noble metal catalyst. Thus, studies focused on strategies to improve their own activity rather than to compare with Pt catalysts. The employed non-noble metals studied included cobalt (Co), copper (Cu), molybdenum (Mo), niobium (Nb), and nickel (Ni).

Co/SiO_2 catalysts prepared using different cobalt precursors were studied for cyclohexane dehydrogenation [98]. The catalytic activity depended on the precursor used as follows: $[Co(bipy)_3](NO_3)_2$> $[Co(NH_3)_5Cl]Cl_2$>$[Co(NH_3)_6]Cl_3$>$[Co(en)_2Cl_2]Cl$. This activity difference was determined by the charge density of cobalt precursors; particularly, $[Co(bipy)_3](NO_3)_2$ afforded the Co/SiO_2 with highly dispersed Co^{2+} species. In case of Cu catalysts, the smaller the Cu particles in Cu/SBA-15, the lower active energy barrier and the higher H_2 evolution rate in cyclohexane dehydrogenation [99]. However, the reaction rate decreased when Cu was smaller than the minimum size. In fact, the H_2 evolution rate of 1 wt% Cu/SBA-15 was half that of 2 wt% Cu/SBA-15 catalyst although Cu particle size was smaller in the former catalyst than in the latter.

Mo and molybdenum carbide (Mo_2C) catalysts are also stud-

Table 3. Examples of other single matal catalysts reported for LOHC dehydrogenation

Active metal	Promotor	Support	Preparation method	Reactant	Reaction temperature (°C)	Reactor type	Results[a]	Ref.
Ir	-	USY	Impregnation	MCH	250	Continuous	X=9.7% at 1 h S to toluene=89% at 1 h	97
Co	-	SiO_2	Strong electrostatic adsorption	Cyclohexane	550	Continuous	TOF=624 h^{-1} S to benzene=45.2% at 80 min	98
Cu	-	SBA-15	Impregnation	Cyclohexane	350	Continuous	5,578 mol_{H2} g_{Cu}^{-1} h^{-1} S to benzene=100%	99
Mo	-	SiO_2	Sol-gel	MCH	400	Continuous	H_2 yield=13% S to toluene=90%	100
	-	MWCNTs	Impregnation	MCH	400	Continuous	3.47 $mmol_{H2}$ h^{-1} m^{-2}	101
Ni	-	Al_2O_3	Impregnation	MCH	440	Continuous	X=9.2%	105
	TiO_2	Al_2O_3	Impregnation	Cyclohexane	300	Batch	~0.08 $mmol_{H2}$ g_{Ni}^{-1} s^{-1}	107
	P	Al_2O_3	Impregnation	Cyclohexane	340	Continuous	TOF=0.139 s^{-1} X=80% Benzene yield=79.9%	108
Raney Ni	-	-	-	MCH	250	Batch	X=~65%	109
Raney Ni	-	-	-	Cyclohexane	322	Continuous	0.20 $mmol_{H2}$ cm^{-2} Ni min^{-1}	110

[a]X=conversion, S=selectivity

ied in MCH dehydrogenation. When Mo-SiO_2 catalysts were synthesized by the sol-gel method, the highest hydrogen generation was achieved at the molar ratio of Mo/Si=0.1 [100]. However, more addition of Mo caused the formation of inactive MoO_3 and unstable Mo species, thus increasing catalyst acidity related with coke formation in Mo-SiO_2. To prevent this deactivation, Li et al. [101] synthesized Mo_2C catalysts using multi-walled carbon nanotubes (MWCNT) subjected to nitric acid treatment producing oxygen functional groups. This method promoted the dispersion of Mo oxyanions and inhibited agglomeration of Mo_2C particles due to the SMSI effect between MWCNT and Mo precursor. The resuling catalyst showed a higher activity than Mo and MoO_2 catalysts in MCH dehydrogenation. In addition, the temperature of carbothermal hydrogen reduction for Mo_2C formation was lower when using MWCNT compared to other carbon supports. Additionally, three-dimensional micron-sized block carbon-molybdenum carbide (BCMC) composite was used for cyclohexane dehydrogenation [102]. BCMC maintained a stable Mo state and excellent activity, while the catalytic performance increased with the Mo amount. The latter result was explained by a decrease in the activation energy of the reaction due to a large amount of high-density Mo_2C inside BCMC.

Another non-noble metal catalyst is niobium oxynitrides (NbON) prepared from niobium oxide [103]. When compared with molybdenum oxynitrides and tungsten oxynitrides, NbON showed better initial activity in cyclohexane dehydrogenation, yet it was less stable when exposed to air due to fast superficial oxidation. Therefore, NbON needs to be free of various stability problems for practical dehydrogenation catalysts.

In the dehydrogenation of homocyclic LOHC, Ni is the most studied non-noble metal and used in types of supported Ni catalysts and Raney Ni. Ni/silica was less active than Pt/Al_2O_3 in cyclohexane dehydrogenation; however, its activity could be optimized at 8 wt% Ni loading [104]. Also, Yolcular et al. [105] found that the activation temperature greatly affected the activity of supported Ni catalysts in MCH dehydrogenation: conversion over 20 wt% Ni/Al_2O_3 was the highest by activation at 723 K. Correlation between Ni particle size of Ni/SiO_2 and surface reactivity (TOF of benzene) was also studied in cyclohexane dehydrogenation [106]. Modeling results demonstrated that the particle size and TOF were inversely proportional to each other in Ni catalysts with Ni particles smaller than 2.5 nm, whereas the particle size and TOF were independent when Ni particles were larger than 2.5 nm. Particularly, there are many low coordination sites on the surface of Ni particles smaller than 2.5 nm, promoting hydrogen desorption and thereby increasing the number of active sites available for the reaction.

To improve the activity of Ni/Al_2O_3, TiO_2 was mixed with Al_2O_3 while Ti composition, Ni loading, and reduction temperature varied [107]. When the prepared Ni/Al_2O_3-TiO_2 catalysts were applied for cyclohexane dehydrogenation, the molar ratio of Al/Ti=25 was found to be the best according to geometrical and electronic effects induced by the apparent SMSI state. Also, 10 wt% Ni was the best loading in terms of Ni^0 particle size. Furthermore, the initial activity increased with the reduction temperature but coke deposition was accelerated, suggesting 773 K as the most appropriate reduction temperature. On the other hand, phosphorous doping to Ni/Al_2O_3 brought about an ensemble effect that is beneficial to cyclohexane dehydrogenation [108]. This modification allowed the transition of Ni to Ni_2P with Ni being electron deficient. This ensemble effect contributed to reduced sintering of Ni particles and enhanced

adsorption of cyclohexane, while weakening benzene adsorption.

Raney Ni was also used in MCH dehydrogenation, where the catalytic activity reached the maximum of about 65% conversion at 523 K [109]. When Raney Ni was applied for cyclohexane dehydrogenation under "wet-dry" multiphase reaction conditions [110], a dehydrogenation reaction happened in the outer layer of catalyst pellet and a strong purging effect occured due to rapid evaporation of orgnic liquids on the catalyst surface.

BIMETALLIC CATALYSTS

1. Pt-containing Bimetallic Catalysts

The approach generally selected to boost the activity of single Pt catalysts in the dehydrogenation of homocyclic LOHC is to prepare bimetallic catalysts in combination of Pt with Rh, Ir, W, Re, Sn, Co, Ni, Cu, Mo, Mn, etc. (Table 4). Major roles of these additives can be categorized in terms of three aspects, such as addition of a new function, geometrical effect, and electronic effect. Since Pt is excellent in C-C bond cleavage, it is imperative to diminish side reactions involving the formation of light alkanes. From this viewpoint, it is necessary to increase Pt dispersion against C-C bond rupture, where the geometrical effect represents this promotion. Also, the electronic effect signifies the change in electron density caused by electron transfer to Pt, affecting Pt-H interaction, reactant adsorption, product desorption, and consequently hydrogen spillover.

In a screening study for cyclohexane dehydrogenation over Pt-containing bimetallic catalysts supported on Al_2O_3, addition of Rh, Ir, and Re showed enhancement in the activity of bare Pt [111]. Notably, Pt-Rh catalyst was the best combination in the dehydro-

Table 4. Examples of Pt-containing bimetallic catalysts reported for LOHC dehydrogenation

Active metal	Promotor	Support	Preparation method	Reactant	Reaction temperature (°C)	Reactor type	Results[a]	Ref.
Pt	Rh	Al_2O_3	Sequential impregnation	Cyclohexane	250 to 350	Continuous	Higher X	111
	Rh	AC	Co-impregnation	Cyclohexane	328	Spray-pulsed	740 $mmol_{H2}$ g_{Pt}^{-1} min^{-1}	112
	Ir	AC	Co-impregnation	Decalin	210	Liquid-film state	30.7 $mmol_{H2}$ for 2.5 h X=32.0% for 2.5 h k=56.8 mmol h^{-1}	38, 39
	W	AC	Dry-migration	Decalin	210	Liquid-film state	35.8 $mmol_{H2}$ for 2.5 h X=37.3% for 2.5 h k=95.2 mmol h^{-1}	38, 39
	Re	Al_2O_3	-	MCH	500	Continuous	X=~100% for 20 h	113
	Re	AC	Sequential impregnation	Cyclohexane	195	Batch	k=2.5 mmol min^{-1} TOF=32 min^{-1}	114
	Re	Al_2O_3	Co-impregnation	MCH	-	Continuous	E_a=51.9 kJ mol^{-1}	118
	Sn	AC	Co-impregnation	Cyclohexane	270 to 300	Continuous	Smaller particle size, but higher E_a	120
	Sn	$MgAl_2O_4$	Sequential impregnation	Cyclohexane	550	Continuous	10.7 $mmol_{H2}$ g_{Pt}^{-1} min^{-1}	121
	Sn	$MgAl_2O_4$	Sequential impregnation	Cyclohexane	550	Continuous	Higher X, S to benzene, and stability	122
	Sn	Mg-Al mixed oxides	Co-impregnation	MCH	300	Continuous	262.1 $mmol_{H2}$ g_{Pt}^{-1} min^{-1} X=90.5% No carbon deposition for 10 h	125
	Ni	Al_2O_3	Co-precipitation	MCH	350	Continuous	X=97.0% S to toluene=~100%	136
	Cu	SiO_2	Co-deposition	Cyclohexane	147 to 377	Continuous	Lower E_a→higher activity	129
	Cu	AC	Impregnation+ transmetallation	Decalin	210	Batch	18.4 $mmol_{H2}$ g_{Pt}^{-1} min^{-1}	131
	Mo	SiO_2	Sol-gel+ impregnation	MCH	400	Continuous	TOF>20,000 h^{-1}	37
	Mn	Al_2O_3	Co-impregnation	MCH	350	Continuous	Higher X, S to toluene, and stability	132

[a]X=conversion, S=selectivity

genation reaction. Kariya et al. [112] reported that the superior activity was ascribed to both electronic promotion and high C-H cleavage ability of Pt-Rh catalyst on active carbon cloth (ACC) sheets. In 5 wt% Pt/C, the activity was improved by addition of Ir and W in decalin dehydrogenation using the superheated liquid-film state [38,39], which is an evidence of bimetallic synergy.

Pt-Re/Al_2O_3 was also proposed as an excellent catalyst in terms of stability and aromatic selectivity because the size of Pt ensembles was smaller than in Pt/Al_2O_3 [113]. The incorporation of Re promoted C-H bond cleavage, electronic effect, and product desorption, resulting in the enhanced activity in MCH dehydrogenation [111,114,115]. However, previous studies explored that the hydrogenolysis activity increased with the addition of Re [116-118]. Considering this conflict, Re induces the dilution of Pt ensemble and advances C-C bond cleavage verified as a reforming catalyst. Alhumaidan et al. [119] reviewed that the kinetics of MCH dehydrogenation would differ by Re addition to Pt/Al_2O_3. It was also reported that Pt-Re catalyst requires an element capable of enhancing both geometric and electron transfer effects for higher selectivity, and that adding an appropriate amount of S can guarantee high activity and selectivity of Pt-Re catalyt.

Pt-Sn catalyst, which is a representative for naphtha reforming, was reported for LOHC dehydrogenation. Pt-Sn/C catalysts were parepared by two synthesis methods, such as co-impregnation (CI) and sequential impregnation (SI) [120]. Although the mean particle size was smaller in Pt-Sn (CI) and larger in Pt-Sn (SI) compared to monometallic Pt, a poor reaction rate and high activation energy were found in cyclohexane dehydrogenation. These unexpected results were caused by blocking of Pt sites by Sn. Considering the absence of Pt-Sn synergy, there was an attempt to use a Sn-modified MgAlO as support for Pt catalyst [121,122]. Microwave calcination enhanced the interaction between Sn and support, and reduced the support acidity; thus, the prepared catalyst showed good dehydrogenation efficiency. However, several side reactions such as disproportionation, demethylation, condensation, ring-opening, and isomerization occurred in MCH dehydrogenation (Fig. 3(a)) [123], which is associated with acidic sites [124]. Thus, Yan et al. [125] modified their previous synthesis method by loading Pt and Sn precursors onto Mg-Al support. Excess Sn suppressed the dehydrogenation activity, while a higher selectivity was achieved by Sn promotion owing to the absence of acidic sites (Fig. 3(b)). Besides, larger pores of this catalyst were beneficial to toluene diffusion, lowering the formation of carbon deposit.

Unlike the negative blocking of Co to Pt catalyst [126], Pt-Ni synergy in C-H bond dissociation and hydrogen desorption was observed in MCH dehydrogenation [127]. Pt-Ni/Al_2O_3 exhibited a

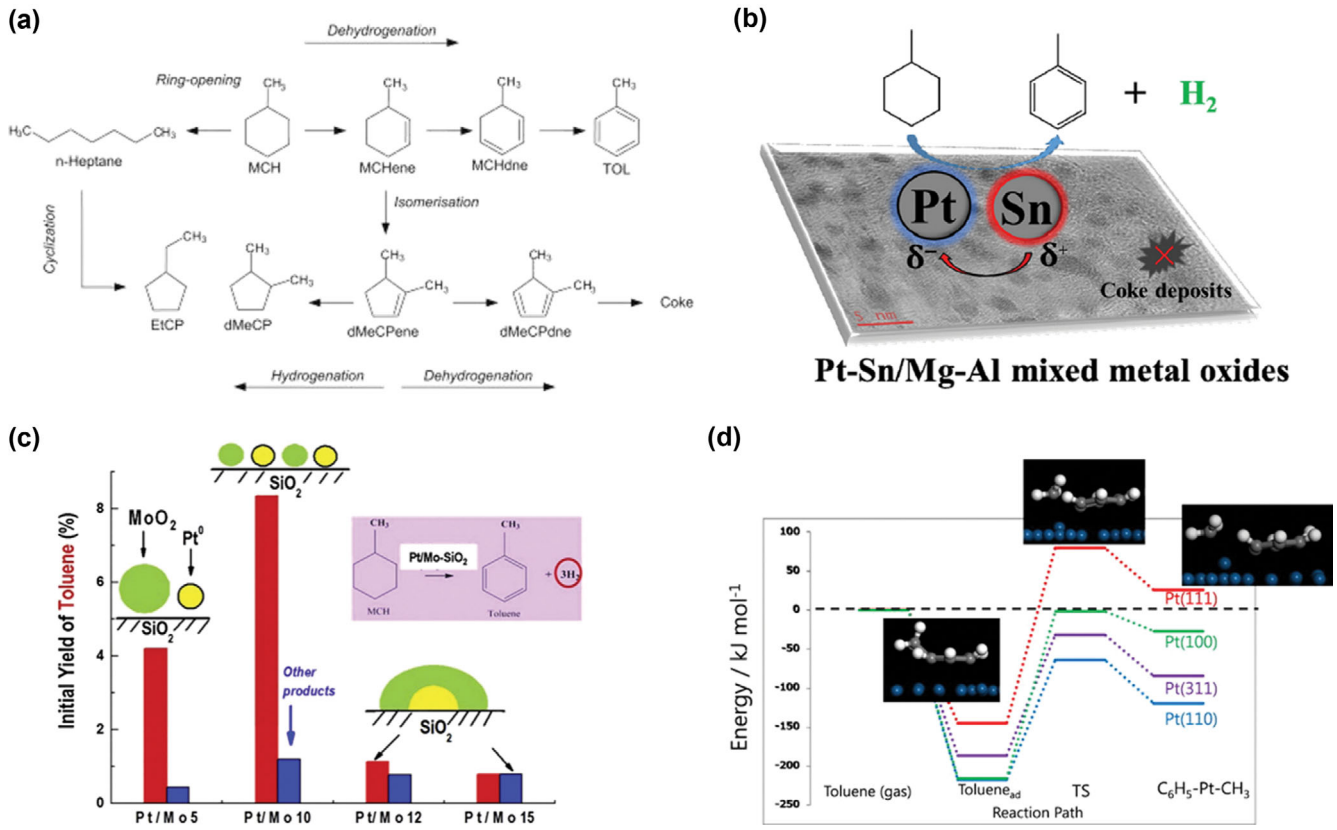

Fig. 3. Key findings of Pt-containing bimetallic catalysts in literature. (a) Reaction pathways to take place during MCH dehydrogenation (Reproduced with permission from Ref. [122], Copyright 2013, Elsevier). (b) Schematic of Pt-Sn/Mg-Al mixed metal oxides for MCH dehydrogenation (Reproduced with permission from Ref. [125], Copyright 2018, Elsevier). (c) Superior activity on partially reduced Pt-Mo/SiO_2 in MCH dehydrogenation (Reproduced with permission from Ref. [124], Copyright 2016, Elsevier). (d) Energy diagram for the demethylation of toluene with respect to Pt facets (Reproduced with permission from Ref. [133], Copyright 2018, Elsevier).

higher conversion than Pt/Al_2O_3 and the improved selectivity with no detection of by-products such as methane by fast toluene desorption. According to DFT study on the mechanism of MCH dehydrogenation for Ni-Pt (111), the activity enhancement originated from the lowered adsorption energy and electron transfer to active Pt species [128].

Cu can be also selected as the second metal. The addition of 0.15 wt% Cu to 1 wt% Pt/SiO_2 reduced the activation energy in cyclohexane dehydrogenation and promoted the activity of Pt/SiO_2 [129]. This result was caused by a change in electron flow in neutral Pt by Cu addition. Furthermore, Pt@Cu/C core-shell catalyst was developed for decalin dehydrogenation [130]. This catalyst showed more hydrogen release of 276 mmol g_{Pt}^{-1} than Pt/C (227 mmol g_{Pt}^{-1}). The beneficial interaction of Pt-Cu was investgated by DFT calculation for such a probe reaction as dehydrogenation of cyclohexane to benzene [131]. As a result, Cu mainly occupied unselective sites of Pt metal, thereby increasing the activity. Also, the benzene selectivty was determined by the energy difference between the barrier of benzene dehydrogenation and benzene desorption. The Cu/Pt (111) was suggested to have the greatest activity among the explored Pt-Cu phases, which will guide the synthesis of more active Pt-Cu catalysts.

Boufaden et al. [124] investigated the catalytic performance of $Pt-Mo/SiO_2$ in MCH dehydrogenation. Higher Mo loadings resulted in poor activity and the formation of MoO_x-Pt core-shell nanoparticles, while the best activity was obtained at 8.0 wt% Mo loading due to high dispersion of MoO_2 and Pt^0 phases (Fig. 3(c)). This indicates that adding an adequate amount of Mo is key to acquiring an active Pt-Mo catalyst. On the other hand, Pt-Mn catalyst was studied to increase H_2 selectivity in MCH dehydrogenation. Sekine et al. [132] reported that $Pt-Mn/Al_2O_3$ had better activity and selectivity than Pt/Al_2O_3 though Pt particle size was similar in

Table 5. Examples of non-Pt containing bimetallic catalysts reported for LOHC dehydrogenation

Active metal	Promotor	Support	Methods of catalyst preparation	Reactant	Reaction temperature (°C)	Reactor type	Results[a]	Ref.
Pd	Te	C	Sequential impregnation	Decalin	250	Liquid-film state	Higher X	95
	Ru	SiCN (silicon carbonitride)	Precursor complex cross-linking	NEC, Perhydro-Phenazine	180, 190	Batch	H_2 yield=95.0% at 20 h, H_2 yield=86.0% at 24 h	134
	Au	rGO	One-pot wet chemical synthesis	NEC	180	Batch	X=~100% at 4 h S to *N*-ethylcarbazole=~100% at 4 h	135
Rh	Ge	Al_2O_3	Redox reaction	Cyclohexane	270	Continuous	6.0 mol_{H2} g_{Rh}^{-1} h^{-1}	136
Rh	Ag	Y_2O_3	Microwave-assisted polyol synthesis	Cyclohexane	300	Spray-pulsed	400.0 $mmol_{H2}$ g_{met}^{-1} min^{-1} 133.3 $mmol_{benzene}$ g_{met}^{-1} min^{-1} X=35.8% for 150 min	137
Ru	Ni	AC	Co-impregnation	Decalin	240	Liquid-film state	Similar to initial rate of Pt/C at 210 °C	138
Ni	Zn	Al_2O_3	Deposition-precipitation	MCH	350	Continuous	X=32.2% S to toluene=96.6%	139
	Zn	Al_2O_3	Deposition-precipitation	MCH	300 to 360	Continuous	Higher TOF	140
	Sn	SiO_2	Chemical vapor deposition (CVD)	Cyclohexane	400	Continuous	Lower X, but higher S to benzene	141
	W	AC	Sequential impregnation	Decalin	400	Continuous	After 22 h, X=93.0% S to naphthalene=99.7%	142
	Cu	SiO_2	Sol-gel	Cyclohexane	350	Continuous	X=94.9% S to benzene=99.5%	143
	Cu	AC	Co-impregnation	MCH	350	Spray-pulsed	39.45 $mmol_{H2}$ g_{met}^{-1} min^{-1} X=25.78% Yield of H_2=19.41%	144
	Cu	SBA-15	Co-impregnation	Cyclohexane	350	Continuous	X=99.4% S to benzene=98.7%	145

[a]X=conversion, S=selectivity

each other. It was found that Pt and Mn were located adjacently without formation of Pt-Mn alloy, while unsaturated sites of Pt (110) and Pt (311) were selectively blocked by Mn (Fig. 3(d)) [133].

2. Non-Pt Containing Bimetallic Catalysts

As listed in Table 5, there are a few reports on bimetallic catalysts composed of other active metals than Pt which is so excellent for the dehydrogenation reaction. As an attractive substitute of Pt, it is important to find non-Pt containing bimetallic catalysts. For this reason, efforts have been made to optimize a combination of two or more different metals and synthesis strategy.

In the dehydrogenation of heterocyclic LOHC, the catalytic activity depends to a large extent on an atomic space group of Pd in the crystal lattice. Thus, a second metal is sometimes added to Pd catalyst. Forberg et al. [134] reported that Pd-Ru catalyst (Pd_2Ru@SiCN) played a signification role in the dehydrogenation of H_{12}-NEC. This bimetallic catalyst exhibited a higher specific reaction rate than Pd@SiCN, resulting in 5.7 wt% of hydrogen release at 180 °C within 20 h. Furthermore, the rGO-supported Pd-M core-shell (M=Au, Ag, Ru, and Rh) bimetallic catalysts were superior to single metal catalysts and their activity followed in the order of $Au_1Pd_{1.3}$ (5.79 wt%)>$Ru_1Pd_{1.3}$ (5.48 wt%)>$Rh_1Pd_{1.3}$ (4.92 wt%)>$Ag_1Pd_{1.3}$ (4.76 wt%) (Fig. 4(a)) [135]. As a result of characterizing surface electronic properties, different core-shell combinations will cause charge transfer between atoms, coverage differences, shift of d-band center, and other changes, thus differing the rate of dehydrogenation reaction.

To improve the activity of Pd/C in decalin dehydrogenation, tellurium (Te) was used for Pd-Te conjugation [95]. In decalin dehydrogenation over liquid-film catalysts, this bimetallic catalyst showed increased performance. Also, Pd catalyst exhibited better activity than Pt in the dehydrogenation of partial aromatic reactants such as phenyl-cyclohexyl, meaning that the molecular property of this reactant is in harmony with Pd catalyst.

Rh-containing bimetallic catalysts were also studied for cyclohexane dehydrogenation, where germanium (Ge) deposition to monometallic Rh catalysts was developed by surface redox reaction [136]. In both Rh-Ge/SiO_2 and Rh-Ge/Al_2O_3, the specific activity was in a volcano-type tendency with the Ge content. Pande et al. [137] prepared Rh-Ag particles supported on Y_2O_3 by microwave-assisted polyol technique. This catalyst was active in cyclohexane dehydrogenation, which results from the Rh-Ag ensemble effect and electron flow change, and also stable during three recycle tests.

Among Ru-containing bimetallic catalysts, Ru-Ni/C prepared by conventional co-impregnation exhibited a higher activity in decalin dehydrogenation, which was achieved by superheated liq-

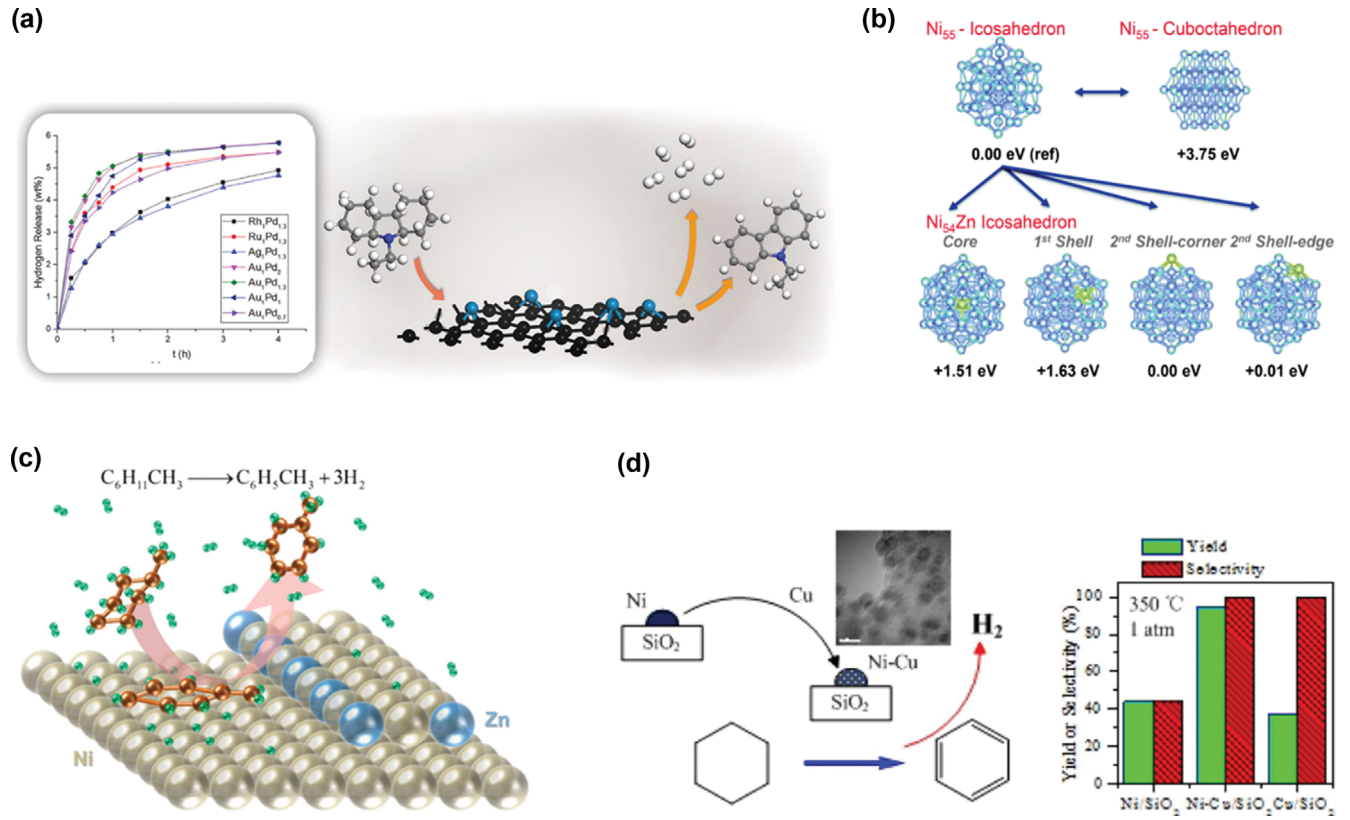

Fig. 4. Key findings of non-Pt containing bimetallic catalysts in literature. (a) Activity results of Pd-M (M=Au, Ag, Ru, Rh) catalysts and schematic of Pd-Au/rGO in H_{12}-NEC dehydrogenation (Reproduced with permission from Ref. [135], Copyright 2019, American Chemical Society). (b) Site preference of Zn replacing one Ni in a Ni_{55} icosahedron cluster (Reproduced with permission from Ref. [139], Copyright 2015, Royal Society of Chemistry). (c) MCH dehydrogenation over the surface of Ni-Zn catalyst (Reproduced with permission from Ref. [140], Copyright 2017, American Chemical Society). (d) Schematic and performance of active Ni-Cu/SiO_2 in cyclohexane dehydrogenation (Reproduced with permission from Ref. [143], Copyright 2016, Elsevier).

uid-film catalysis [138]. This catalyst at 240 °C was comparable to Pt catalyst at 210 °C. In spite of using a slightly higher reaction temperature, the Ru-Ni catalyst was considered to have significant potential in terms of Pt replacement.

Ni-based bimetallic catalysts have been often studied because the C-H bond cleavage ability of Ni is not as outstanding as Pt but is better than other common metals. In the study of bimetallic Ni-Ag, Ni-Zn, Ni-Sn, and Ni-In catalysts for selective MCH dehydrogenation, Ni-Zn/Al_2O_3 achieved the higher selectivity (96.6%) and similar conversion (32.2%) compared to Ni/Al_2O_3 (conversion of 36.2% and selectivity of 66.9%), although the activity was lower than that of Pt/Al_2O_3 along with the selectivity comparable [139]. Regarding the promoted effect of Zn, DFT calculation indicated that Zn was preferentially adsorbed to low-coordinated Ni sites favoring C-C bond cleavage (Fig. 4(b)). Although the dehydrogenation product H_2 is competitively adsorbed on the catalyst surface [65], the kinetic and computational results confirmed that Ni-based catalysts had half a positive order with H_2 pressure, whereas almost zero order appeared with the Pt catalyst. This phenomenon, referred to as hydrogen-assisted desorption, is caused by the C-C bond rupture from defect sites (such as corner and edge sites) of metallic Ni. Unless hydrogen-assisted desorption of intermediate originating from toluene works well, the adsorbed molecules keep the overall reaction to be interfered. To prevent this problem, it is necessary to block Ni defect sites, which could be sufficiently performed by Zn (Fig. 4(c)) [140].

Fine particles of Ni-Sn intermetallic compounds were synthesized by CVD method on SiO_2 support [141]. The average particle diameter was about 3-4 nm and gradually grew with increasing the Sn content. In cyclohexane dehydrogenation, catalytic performance ranked in the order of Ni>Ni_3Sn>Ni_3Sn_2>Ni_3Sn_4. Despite slight decrease in the activity by the addition of Sn, benzene selectivity was rather improved. It was also proposed that Ni-tungsten carbide (WC) catalyst could replace Ni-Pt catalyst [142]. This was based on the calculated hydrogen bonding energy (HBE) associated with the ability to activate C-H bond: Ni-WC site has a similar HBE to Ni-Pt-Pt surface. In actual tests, Ni-WC/AC maintained higher activity than Ni/AC and WC/AC for 22 h in decalin dehydrogenation.

A highly selective dehydrogenation of cyclohexane was achieved with Ni-Cu/SiO_2 synthesized by sol-gel method [143]. Ni/SiO_2 catalyst presented the highest conversion of cyclohexane and the lowest selectivity at 350 °C (Fig. 4(d)), because Ni generally contains better cleavage ability of C-H and C-C bonds than Cu due to the partially filled d-band of Ni [144]. Therefore, based on the Sabatier principle, an appropriate interaction is essential to improve catalytic activity, which was accomplished by Cu addition to Ni catalyst. Actually, the best Ni-Cu/SiO_2 exhibited 94.9% conversion and 99.5% selectivity under the same conditions with Ni/SiO_2. This Cu promotion effect was confirmed in ACC and SBA-15 supports, although the optimized Ni : Cu mole ratio was slightly different [144,145].

CONCLUSIONS AND PERSPECTIVES

LOHC is a hydrogen storage technology with high potential. However, it still needs a breakthrough in the dehydrogenation of heterocyclic and homocyclic molecules. Because of endothermicity, the reaction temperature should be higher: particularly, more severe conditions are required for homocyclic LOHC due to higher reaction enthalpy. The fundamental way to reduce the dehydrogenation enthalpy is the incorporation of heteroatoms into the molecular structure, resulting in fast reaction rate at low temperatures of below 250 °C. However, there are limitations in the synthesis of various heterocyclic molecules, aside from chemical reversibility, stability, and cost. Therefore, catalyst development is crucial for both heterocyclic and homocyclic LOHC. Fig. 5 displays a schematic representing major keys of reactants and catalysts contributing to the efficiency of H_2 release from various LOHC molecules.

Pt is widely used in the dehydrogenation of homocyclic LOHC,

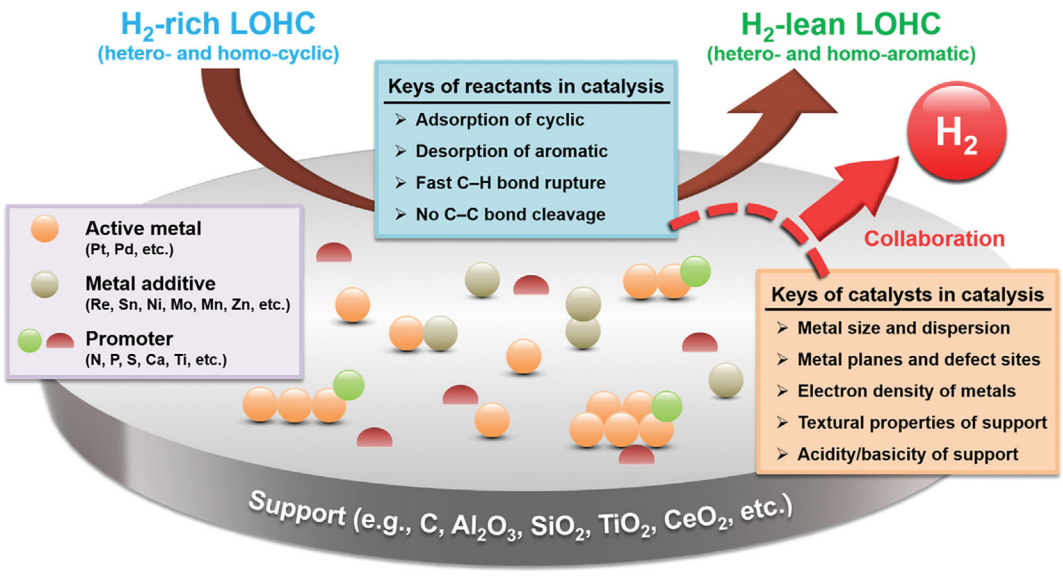

Fig. 5. Schematic representing major keys of reactants and catalysts in dehydrogenation catalysis for LOHC molecules.

whereas Pt tends to be less favored in heterocyclic dehydrogenation due to side reactions (e.g., disproportionation, dealkylation, and C-heteroatom bond cleavage) caused by superior performance of Pt. In catalytic and computational works involving Pd catalyst, Pd (111) plane is very important in obtaining excellent activity in the dehydrogenation of heterocyclic LOHC. Therefore, one needs to explore a synthesis strategy to generate a large number of Pd (111) surfaces in catalyst body.

For homocyclic LOHC, upgrading catalyst properties is the only means to overcome the hurdle of dehydrogenation if ordinary catalytic reactors are employed. Among single metal catalysts, Pt shows excellent C-H bond cleavage. A variety of approaches such as tuning metal particle size and phase optimization, modifying support material, and finding a new synthesis method have been reported. The optimum of metal particle size would differ depending on the metal's ability in cleavage of C-H and C-C bonds, but most of the works show a volcano-type relationship with the metal size. The dehydrogenation efficiency of metal atoms varies differently from the minimum particle size with high intrinsic activity different for each metal. In addition to this ensemble effect, the acid and base properties, and metal-support interaction can be changed by support modification, leading to significant variation in the dehydrogenation performance. The synthesis method is also an interesting approach to control the particle size, phase, and metal-support interaction that are the main characteristics of single metal catalysts.

To meet all the requirements for dehydrogenation, bimetallic catalyst is worth studying. The role of metal additives can be largely divided into three categories: electronic effect, geometric effect, and blocking effect on a main active metal. As found in single metal catalysts, Pt is the most studied main active metal in bimetallic catalysts to dehydrogenate homocyclic LOHC. Among the metals showing synergy with Pt, the electronic effect appearing in Rh, Ir, Re, Ni, and Cu, leads to enhanced C-H cleavage or product desorption. The geometric effect was induced by Re, Sn, and others, where the efficiency of Pt atoms was improved by dilution of the Pt crystal structure. Since Pt generally shows good performance in C-C bond cleavage, the decrease of Pt ensemble would suppress the aforementioned side reactions. Meanwhile, Cu and Mn tend to be adsorbed to unsaturated sites of Pt, which is associated with increases in reaction efficiency and H_2 selectivity. The side reactions are induced by strong adsorption of aromatic products to Pt, C-C bond rupture, and defect sites (i.e., unsaturated coordinates) of Pt. In Pt-containing bimetallic catalysts, metal additives improving these factors also reduced the generation of coke on the catalyst surface, greatly contributing to catalyst stability. In the case of non-Pt containing bimetallic catalysts, there are few studies to investigate their geometrical effect on catalytic performance. However, the electronic effect was investigated in Rh-Ag and Ni-Cu catalysts, the blocking effect was confirmed in Ni-Zn catalyst.

The ultimate target in the dehydrogenation reaction is identical for both homocyclic and heterocyclic LOHC, that is, maximum activity and perfect selectivity. The dehydrogenation mechanism consists of reactant adsorption, surface reaction, and product desorption. Reactant adsorption to active metals should occur strongly, but product desorption would be weak for fast desorption. During the surface reaction, C-H bond cleavage proceeds well with almost no side reactions caused by cleavage of other bonds, including C-C bond. Therefore, active metals of suitable adsorption strength are vital in LOHC dehydrogenation when considering electronic and geometric effects of single metals and bimetals, which is called the Sabatier principle. In this respect, DFT calculation will be helpful in understanding experimentally observed catatalytic actions and catalyst design. Moreover, it is indispensable to identify the effects of the factors mentioned above on each reaction step. Aside from catalytic activity, H_2 purity (i.e., reaction selectivity) and catalyst stability should be considered for catalyst selection. Since an active and stable dehydrogenation catalyst is a key to the realization of LOHC technology, various attempts will be endeavored for precise tuning of active metals, appropriate incorporation of promoters and metal additives, and elegant support modification.

ACKNOWLEDGEMENTS

This work was financially supported by the National Research Foundation of Korea (NRF) funded by the Ministry of Science and ICT, Republic of Korea (NRF-2019M3E6A1064908), and by the Ministry of Education, Republic of Korea (NRF-2016R1A6A1A03013422).

REFERENCES

1. R. York, *Nat. Clim. Change*, **2**, 441 (2012).
2. D.-H. Lee and C.-P. Hung, *Int. J. Hydrogen Energy*, **37**, 15753 (2012).
3. M. G. Schultz, T. Diehl, G. P. Brasseur and W. Zittel, *Science*, **302**, 624 (2003).
4. D. Teichmann, W. Arlt, P. Wasserscheid and R. Freymann, *Energy Environ. Sci.*, **4**, 2767 (2011).
5. G. W. Crabtree, M. S. Dresselhaus and M. V. Buchanan, *Phys. Today*, **57**, 39 (2004).
6. J. Kaldellis, D. Zafirakis and K. Kavadias, *Renew. Sustain. Energy Rev.*, **13**, 378 (2009).
7. I. Jain, *Int. J. Hydrogen Energy*, **34**, 7368 (2009).
8. M. Reuß, T. Grube, M. Robinius, P. Preuster, P. Wasserscheid and D. Stolten, *Appl. Energy*, **200**, 290 (2017).
9. J. Yang, A. Sudik, C. Wolverton and D. J. Siegel, *Chem. Soc. Rev.*, **39**, 656 (2010).
10. H. Wang, X. Zhou and M. Ouyang, *Int. J. Hydrogen Energy*, **41**, 18062 (2016).
11. E. Y. Marrero-Alfonso, A. M. Beaird, T. A. Davis and M. A. Matthews, *Ind. Eng. Chem. Res.*, **48**, 3703 (2009).
12. J. Ren, N. M. Musyoka, H. W. Langmi, M. Mathe and S. Liao, *Int. J. Hydrogen Energy*, **42**, 289 (2017).
13. M. Niermann, A. Beckendorff, M. Kaltschmitt and K. Bonhoff, *Int. J. Hydrogen Energy*, **44**, 6631 (2019).
14. T. Schildhauer, E. Newson and S. Müller, *J. Catal.*, **198**, 355 (2001).
15. K. Müller, K. Stark, V. N. Emel'yanenko, M. A. Varfolomeev, D. H. Zaitsau, E. Shoifet, C. Schick, S. P. Verevkin and W. Arlt, *Ind. Eng. Chem. Res.*, **54**, 7967 (2015).
16. K. M. Eblagon and S. E. Tsang, *Appl. Catal. B-Environ.*, **163**, 599 (2015).

17. R. K. Ahluwalia, T. Q. Hua and J. K. Peng, *Int. J. Hydrogen Energy*, **37**, 2891 (2012).
18. F. Sotoodeh, B. J. M. Huber and K. J. Smith, *Appl. Catal. A-Gen.*, **419-420**, 67 (2012).
19. G. E. Dobereiner, A. Nova, N. D. Schley, N. Hazari, S. J. Miller, O. Eisenstein and R. H. Crabtree, *J. Am. Chem. Soc.*, **133**, 7547 (2011).
20. R. H. Crabtree, *ACS Sustain. Chem. Eng.*, **5**, 4491 (2017).
21. K. Müller, J. Völkl and W. Arlt, *Energy Technol.*, **1**, 20 (2013).
22. K. M. Eblagon, D. Rentsch, O. Friedrichs, A. Remhof, A. Zuettel, A. Ramirez-Cuesta and S. C. Tsang, *Int. J. Hydrogen Energy*, **35**, 11609 (2010).
23. K. M. Eblagon, K. Tam, K. K. Yu, S.-L. Zhao, X.-Q. Gong, H. He, L. Ye, L.-C. Wang, A. J. Ramirez-Cuesta and S. C. Tsang, *J. Phys. Chem. C*, **114**, 9720 (2010).
24. K. Stark, P. Keil, S. Schug, K. Müller, P. Wasserscheid and W. Arlt, *J. Chem. Eng. Data*, **61**, 1441 (2016).
25. N. Heublein, M. Stelzner and T. Sattelmayer, *Int. J. Hydrogen Energy*, **45**, 24902 (2020).
26. M. Geißelbrecht, S. Mrusek, K. Müller, P. Preuster, A. Bösmann and P. Wasserscheid, *Energy Environ. Sci.*, **13**, 3119 (2020).
27. J. Oh, K. Jeong, T. W. Kim, H. Kwon, J. W. Han, J. H. Park and Y.-W. Suh, *ChemSusChem*, **11**, 661 (2018).
28. B. Wang, Y.-T. Chen, T.-Y. Chang, Z. Jiang, Z.-Q. Huang, S.-Y. Wang, C.-R. Chang, Y.-S. Chen, J.-J. Wei, S. Yang and T. Fang, *Appl. Catal. B-Environ.*, **266**, 118658 (2020).
29. E. Gianotti, M. Taillades-Jacquin, J. Rozière and D. J. Jones, *ACS Catal.*, **8**, 4660 (2018).
30. P. T. Aakko-Saksa, C. Cook, J. Kiviaho and T. Repo, *J. Power Sources*, **396**, 803 (2018).
31. L. Zhou, L. Sun, L. Xu, C. Wan, Y. An and M. Ye, *Catalysts*, **10**, 648 (2020).
32. P. C. Rao and M. Yoon, *Energies*, **13**, 6040 (2020).
33. H. Yook, K. Kim, J. H. Park, Y.-W. Suh and J. W. Han, *Catal. Today*, **352**, 345 (2020).
34. K. Kim, J. Oh, T. W. Kim, J. H. Park, J. W. Han and Y.-W. Suh, *Catal. Sci. Technol.*, **7**, 3728 (2017).
35. M. Niermann, S. Drünert, M. Kaltschmitt and K. Bonhoff, *Energy Environ. Sci.*, **12**, 290 (2019).
36. P. D. Vaidya and A. E. Rodrigues, *Chem. Eng. Tech.*, **32**, 1463 (2009).
37. S. N. Delgado, D. Yap, L. Vivier and C. Especel, *J. Mol. Catal. A-Chem.*, **367**, 89 (2013).
38. N. Jiang, K. R. Rao, M.-J. Jin and S.-E. Park, *Appl. Catal. A-Gen.*, **425**, 62 (2012).
39. S. Hodoshima, H. Arai and Y. Saito, *Int. J. Hydrogen Energy*, **28**, 197 (2003).
40. S. Hodoshima, H. Arai, S. Takaiwa and Y. Saito, *Int. J. Hydrogen Energy*, **28**, 1255 (2003).
41. C. Shinohara, S. Kawakami, T. Moriga, H. Hayashi, S. Hodoshima, Y. Saito and S. Sugiyama, *Appl. Catal. A-Gen.*, **266**, 251 (2004).
42. S. Hodoshima, S. Takaiwa, A. Shono, K. Satoh and Y. Saito, *Appl. Catal. A-Gen.*, **283**, 235 (2005).
43. X. Li, Y. Tuo, P. Li, X. Duan, H. Jiang and X. Zhou, *Carbon*, **67**, 775 (2014).
44. G. Lee, J. Y. Kang, Y. Jeong and J. C. Jung, *Korean J. Mater. Res.*, **25**, 191 (2015).
45. C. Zhang, X. Liang and S. Liu, *Int. J. Hydrogen Energy*, **36**, 8902 (2011).
46. P. Li, Y.-L. Huang, D. Chen, J. Zhu, T.-J. Zhao and X.-G. Zhou, *Catal. Commun.*, **10**, 815 (2009).
47. Q. Zhou, P. Li, X. Wang, X. Zhou, D. Yang and D. Chen, *Mat. Chem. Phys.*, **126**, 41 (2011).
48. Y. Tuo, H. Jiang, X. Li, L. Shi, X. Yu and P. Li, *Int. J. Hydrogen Energy*, **41**, 10755 (2016).
49. G. Lee, Y. Jeong, B.-G. Kim, J. S. Han, H. Jeong, H. B. Na and J. C. Jung, *Catal. Commun.*, **67**, 40 (2015).
50. M. Lazaro, E. Garcia-Bordeje, D. Sebastian, M. Lazaro and R. Moliner, *Catal. Today*, **138**, 203 (2008).
51. D. Sebastián, E. Bordejé, L. Calvillo, M. Lázaro and R. Moliner, *Int. J. Hydrogen Energy*, **33**, 1329 (2008).
52. K. Nakagawa, T. Okayama, Y. Tanimoto, K.-I. Sotowa, S. Sugiyama, T. Moriga, S. Takenaka and M. Kishida, *Appl. Catal. A-Gen.*, **419**, 13 (2012).
53. X. Wang, N. Li, J. A. Webb, L. D. Pfefferle and G. L. Haller, *Appl. Catal. B-Environ.*, **101**, 21 (2010).
54. Y. Tuo, X. Liu, L. Shi, L. Yang, P. Li and W. Yuan, *Catal. Today*, **347**, 87 (2020).
55. Y. Tuo, L. Yang, X. Ma, Z. Ma, S. Gong and P. Li, *Int. J. Hydrogen Energy*, **46**, 930 (2021).
56. J. Wang, H. Liu, S. Fan, W. Li, Z. Li, H. Yun, X. Xu, A. Guo and Z. Wang, *Energy Fuels*, **34**, 16542 (2020).
57. X. Sha, M. T. Knippenberg, A. C. Cooper, G. P. Pez and H. Cheng, *J. Phys. Chem. C*, **112**, 17465 (2008).
58. J. C. Araújo, L. F. Oton, A. C. Oliveira, R. Lang, L. Otubo and J. M. Bueno, *Int. J. Hydrogen Energy*, **44**, 27329 (2019).
59. J. Yu, Q. Ge, W. Fang and H. Xu, *Appl. Catal. A-Gen.*, **395**, 114 (2011).
60. J. Yu, Q. Ge, W. Fang and H. Xu, *Int. J. Hydrogen Energy*, **36**, 11536 (2011).
61. F. Auer, D. Blaumeiser, T. Bauer, A. Bösmann, N. Szesni, J. Libuda and P. Wasserscheid, *Catal. Sci. Technol.*, **9**, 3537 (2019).
62. F. Auer, A. Hupfer, A. Bösmann, N. Szesni and P. Wasserscheid-peter, *Catal. Sci. Technol.*, **10**, 6669 (2020).
63. L. Shi, Y. Zhou, S. Qi, K. J. Smith, X. Tan, J. Yan and C. Yi, *ACS Catal.*, **10**, 10661 (2020).
64. X. Yang, Y. Song, T. Cao, L. Wang, H. Song and W. Lin, *Mol. Catal.*, **492**, 110971 (2020).
65. S. Nagatake, T. Higo, S. Ogo, Y. Sugiura, R. Watanabe, C. Fukuhara and Y. Sekine, *Catal. Lett.*, **146**, 54 (2016).
66. Y. Sugiura, T. Nagatsuka, K. Kubo, Y. Hirano, A. Nakamura, K. Miyazawa, Y. Iizuka, S. Furuta, H. Iki and T. Higo, *Chem. Lett.*, **46**, 1601 (2017).
67. M. Kosaka, T. Higo, S. Ogo, J.G. Seo, S. Kado, K.-i. Imagawa and Y. Sekine, *Int. J. Hydrogen Energy*, **45**, 738 (2020).
68. K. Takise, A. Sato, K. Murakami, S. Ogo, J. G. Seo, K.-i. Imagawa, S. Kado and Y. Sekine, *RSC Adv.*, **9**, 5918 (2019).
69. M. Bonne, P. Samoila, T. Ekou, C. Especel, F. Epron, P. Marécot, S. Royer and D. Duprez, *Catal. Commun.*, **12**, 86 (2010).
70. A. Chen, W. Zhang, X. Li, D. Tan, X. Han and X. Bao, *Catal. Lett.*, **119**, 159 (2007).
71. C. Xiao, R. V. Maligal-Ganesh, T. Li, Z. Qi, Z. Guo, K. T. Brashler, S. Goes, X. Li, T. W. Goh and R. E. Winans, *ChemSusChem*, **6**, 1915 (2013).

72. S. Lee, J. Lee, T. Kim, G. Han, J. Lee, K. Lee and J. Bae, *Int. J. Hydrogen Energy*, **46**, 5520 (2021).
73. A. A. Shukla, P. V. Gosavi, J. V. Pande, V. P. Kumar, K. V. Chary and R. B. Biniwale, *Int. J. Hydrogen Energy*, **35**, 4020 (2010).
74. A. Shukla, J. V. Pande and R. B. Biniwale, *Int. J. Hydrogen Energy*, **37**, 3350 (2012).
75. X. Gong, Z. Jiang and T. Fang, *Int. J. Hydrogen Energy*, **45**, 6838 (2020).
76. T. N. Phan, Y.-K. Park, I.-G. Lee and C. H. Ko, *Appl. Catal. A-Gen.*, **544**, 84 (2017).
77. W. Peters, A. Seidel, S. Herzog, A. Bösmann, W. Schwieger and P. Wasserscheid, *Energy Environ. Sci.*, **8**, 3013 (2015).
78. D. Dean, B. Davis and P. G. Jessop, *New J. Chem.*, **35**, 417 (2011).
79. M. Yang, Y. Dong, S. Fei, H. Ke and H. Cheng, *Int. J. Hydrogen Energy*, **39**, 18976 (2014).
80. F. Sotoodeh and K. J. Smith, *J. Catal.*, **279**, 36 (2011).
81. F. Sotoodeh, B. J. Huber and K. J. Smith, *Int. J. Hydrogen Energy*, **37**, 2715 (2012).
82. B. Wang, T. Yan, T. Chang, J. Wei, Q. Zhou, S. Yang and T. Fang, *Carbon*, **122**, 9 (2017).
83. Z. Feng, X. Chen and X. Bai, *Environ. Sci. Pollut. Res.*, **27**, 36172 (2020).
84. T. Hara, K. Mori, T. Mizugaki, K. Ebitani and K. Kaneda, *Tetrahedron Letters*, **44**, 6207 (2003).
85. S. Sugiyama, T. Minami, H. Hayashi, M. Tanaka, N. Shigemoto and J. B. Moffat, *J. Chem. Soc. Faraday Trans.*, **92**, 293 (1996).
86. P. Nikulshin, V. Salnikov, A. Mozhaev, P. Minaev, V. Kogan and A. Pimerzin, *J. Catal.*, **309**, 386 (2014).
87. J. Oh, T. W. Kim, K. Jeong, J. H. Park and Y.-W. Suh, *ChemCatChem*, **10**, 3892 (2018).
88. J. Oh, H. B. Bathula, J. H. Park and Y.-W. Suh, *Commun. Chem.*, **2**, 68 (2019).
89. H. B. Bathula, J. Oh, Y. Jo and Y.-W. Suh, *Catalysts*, **9**, 719 (2019).
90. S. Yoon, K. Oh, F. Liu, J. H. Seo, G. A. Somorjai, J. H. Lee and K. An, *ACS Catal.*, **8**, 5391 (2018).
91. F. Sotoodeh, L. Zhao and K. J. Smith, *Appl. Catal. A-Gen.*, **362**, 155 (2009).
92. E. A. Monyoncho, S. Ntais, N. Brazeau, J. J. Wu, C. L. Sun and E. A. Baranova, *ChemElectroChem*, **3**, 218 (2016).
93. W.-J. Shen, M. Okumura, Y. Matsumura and M. Haruta, *Appl. Catal. A-Gen.*, **213**, 225 (2001).
94. Y. Kim, Y. Song, Y. Choi, K. Jeong, J. H. Park, K. C. Ko and K. Na, *ACS Sustain. Chem. Eng.*, **9**, 809 (2021).
95. W. Ninomiya, Y. Tanabe, K.-I. Sotowa, T. Yasukawa and S. Sugiyama, *Res. Chem. Intermed.*, **34**, 663 (2008).
96. R. Schuster, F. Waidhas, M. Bertram, H. Runge, S. Geile, R. Shayduk, M. Abuín, V. Vonk, H. Noei, Y. Lykhach, F. Bertram, A. Stierle and J. Libuda, *Catal. Lett.*, **148**, 2901 (2018).
97. D. K. Cromwell, P. T. Vasudevan, B. Pawelec and J. L. G. Fierro, *Catal. Today*, **259**, 119 (2016).
98. K. Choojun, A. Worathanaseth, S. Kuhatasanadeekul, T. Kurato, S. Ketaniruj, P. Phichitsurathaworn, P. Promchana, K. Prakobtham, N. Numwong and Y. Poo-arporn, *Catal. Commun.*, **125**, 108 (2019).
99. Z. Xia, H. Liu, H. Lu, Z. Zhang and Y. Chen, *Catal. Lett.*, **147**, 1295 (2017).
100. N. Boufaden, R. Akkari, B. Pawelec, J. Fierro, M. S. Zina and A. Ghorbel, *Appl. Catal. A-Gen.*, **502**, 329 (2015).
101. X. Li, D. Ma, L. Chen and X. Bao, *Catal. Lett.*, **116**, 63 (2007).
102. H. Wang, N. Zhang, R. Liu, R. Zhao, T. Guo, J. Li, T. Asefa and J. Du, *ACS Omega*, **3**, 10773 (2018).
103. R. Brayner, J. Rodrigues and G. Cruz, *Catal. Today*, **57**, 219 (2000).
104. H. M. Gobara and M. M. Gomaa, *Petro. Sci. Tech.*, **27**, 1572 (2009).
105. S. Yolcular and Ö. Olgun, *Catal. Today*, **138**, 198 (2008).
106. Y. Yao, Z. Yan, L. Chen, Z. Zhou, L. Liu and D. W. Goodman, *Catal. Lett.*, **142**, 1437 (2012).
107. J. Escobar, J. A. De Los Reyes, T. Viveros and M. C. Barrera, *Ind. Eng. Chem. Res.*, **45**, 5693 (2006).
108. J. Li, Y. Chai, B. Liu, Y. Wu, X. Li, Z. Tang, Y. Liu and C. Liu, *Appl. Catal. A-Gen.*, **469**, 434 (2014).
109. L. Zhang, G. Xu, Y. An, C. Chen and Q. Wang, *Int. J. Hydrogen Energy*, **31**, 2250 (2006).
110. Z. Kou, Z. Zhi, G. Xu, Y. An and C. He, *Appl. Catal. A-Gen.*, **467**, 196 (2013).
111. L. I. Ali, A.-G. A. Ali, S. Aboul-Fotouh and A. K. Aboul-Gheit, *Appl. Catal. A-Gen.*, **177**, 99 (1999).
112. N. Kariya, A. Fukuoka, T. Utagawa, M. Sakuramoto, Y. Goto and M. Ichikawa, *Appl. Catal. A-Gen.*, **247**, 247 (2003).
113. W. J. Doolittle, N. D. Skoularikis and R. W. Coughlin, *J. Catal.*, **107**, 490 (1987).
114. J. K. Hoyano and W. A. Graham, *J. Am. Chem. Soc.*, **104**, 3722 (1982).
115. N. Kariya, A. Fukuoka and M. Ichikawa, *Appl. Catal. A-Gen.*, **233**, 91 (2002).
116. P. Biloen, J. Helle, H. Verbeek, F. Dautzenberg and W. Sachtler, *J. Catal.*, **63**, 112 (1980).
117. L. Jossens and E. Petersen, *J. Catal.*, **76**, 265 (1982).
118. K. Jothimurugesan, S. Bhatia and R. D. Srivastava, *Ind. Eng. Chem. Fundam.*, **24**, 433 (1985).
119. F. Alhumaidan, D. Cresswell and A. Garforth, *Energy Fuels*, **25**, 4217 (2011).
120. M. C. Román-Martínez, J. A. Macia-Agullo, I. M. J. Vilella, D. Cazorla-Amorós and H. Yamashita, *J. Phys. Chem. C*, **111**, 4710 (2007).
121. N.-l. Wang, J.-e. Qiu, Z.-w. Wu, J. Wu, K.-y. You and H.-a. Luo, *Appl. Catal. A-Gen.*, **503**, 62 (2015).
122. N. Wang, J. Wu, X. Yuan, K. You and H. a. Luo, *Appl. Catal. A-Gen.*, **516**, 9 (2016).
123. F. Alhumaidan, D. Tsakiris, D. Cresswell and A. Garforth, *Int. J. Hydrogen Energy*, **38**, 14010 (2013).
124. N. Boufaden, R. Akkari, B. Pawelec, J. Fierro, M. S. Zina and A. Ghorbel, *J. Mol. Catal. A-Chem.*, **420**, 96 (2016).
125. J. Yan, W. Wang, L. Miao, K. Wu, G. Chen, Y. Huang and Y. Yang, *Int. J. Hydrogen Energy*, **43**, 9343 (2018).
126. P. Tétényi and V. Galsán, *Appl. Catal. A-Gen.*, **229**, 181 (2002).
127. F. Wang, Y. Q. Yang and W. Y. Wang, *Adv. Mat. Res.*, **881**, 315 (2014).
128. C. Mi, Y. Huang, F. Chen, K. Wu, W. Wang and Y. Yang, *Int. J. Hydrogen Energy*, **46**, 875 (2021).
129. N. Galimova, Z. Pskhu, A. Naumkin, I. Volkov, T. Yagodovskaya, E. Platonov and V. Yagodovskii, *Russ. J. Phys. Chem. A*, **84**, 1908 (2010).

130. S. C. Feng, H. Y. Ma and P. P. Hao, *J. Mol. Model.*, **26**, 89 (2020).
131. J. Y. Kang, G. Lee, Y. Jeong, H. B. Na and J. C. Jung, *Korean J. Mater. Res.*, **26**, 17 (2016).
132. A. Nakano, S. Manabe, T. Higo, H. Seki, S. Nagatake, T. Yabe, S. Ogo, T. Nagatsuka, Y. Sugiura and H. Iki, *Appl. Catal. A-Gen.*, **543**, 75 (2017).
133. S. Manabe, T. Yabe, A. Nakano, S. Nagatake, T. Higo, S. Ogo, H. Nakai and Y. Sekine, *Chem. Phys. Lett.*, **711**, 73 (2018).
134. D. Forberg, T. Schwob, M. Zaheer, M. Friedrich, N. Miyajima and R. Kempe, *Nat. Commun.*, **7**, 13201 (2016).
135. B. Wang, T.-y. Chang, X. Gong, Z. Jiang, S. Yang, Y.-s. Chen and T. Fang, *ACS Sustain. Chem. Eng.*, **7**, 1760 (2019).
136. G. Lafaye, C. Micheaud-Especel, C. Montassier and P. Marecot, *Appl. Catal. A-Gen.*, **230**, 19 (2002).
137. J. V. Pande, A. B. Bindwal, Y. B. Pakade and R. B. Biniwale, *Int. J. Hydrogen Energy*, **43**, 7411 (2018).
138. S. Hodoshima, H. Nagata and Y. Saito, *Appl. Catal. A-Gen.*, **292**, 90 (2005).
139. A. H. Al-ShaikhAli, A. Jedidi, L. Cavallo and K. Takanabe, *Chem. Commun.*, **51**, 12931 (2015).
140. A. H. Al-ShaikhAli, A. Jedidi, D. H. Anjum, L. Cavallo and K. Takanabe, *ACS Catal.*, **7**, 1592 (2017).
141. A. Onda, T. Komatsu and T. Yashima, *J. Catal.*, **221**, 378 (2004).
142. S. Qi, J. Yue, Y. Li, J. Huang, C. Yi and B. Yang, *Catal. Lett.*, **144**, 1443 (2014).
143. Z. Xia, H. Lu, H. Liu, Z. Zhang and Y. Chen, *Catal. Commun.*, **90**, 39 (2017).
144. S. P. Patil, J. V. Pande and R. B. Biniwale, *Int. J. Hydrogen Energy*, **38**, 15233 (2013).
145. M. Wojciechowska, I. Tomska-Foralewska, W. Przystajko and M. Zieliński, *Catal. Lett.*, **104**, 121 (2005).

Young-Woong Suh obtained B.S. degree in Chemical Engineering from Hanyang University, Korea, in 1997, and received M.S. and Ph.D. degrees in Chemical Engineering from Seoul National University, Korea, in 1999 and 2003, respectively. From 2003 to 2006, he was a postdoctoral research associate at Northwestern University. He worked as a senior research scientist at the Korea Institute of Science and Technology until 2011. Then, he joined Hanyang University in 2011 and is currently a full professor in the Department of Chemical Engineering. He has published over 120 manuscripts in SCI journals, and 30 international and domestic patents. His research interests are in the area of heterogeneous catalysis including biomass conversion, chemical hydrogen storage, environmentally-friendly catalytic processing.

Joon Hyun Baik obtained B.S. degree in Chemical Engineering from Hanyang University, Korea, in 2001. He received M.S. and Ph.D. degrees in Chemical Engineering from Pohang University of Science and Technology (POSTECH), Korea, in 2003 and 2007, respectively. From 2007 to 2009, he was a postdoctoral fellow at MIT and Pennsylvania State University. He worked at Research Institute of Industrial Science and Technology (RIST) as senior researcher for 11 years from 2009 to 2020. He is currently an assistant professor in Department of Chemical & Biological Engineering of Sookmyung Women's University. He has 37 papers and 38 patents regarding environmental catalysis, CO_2 utilization, and catalytic hydrogenation technologies.